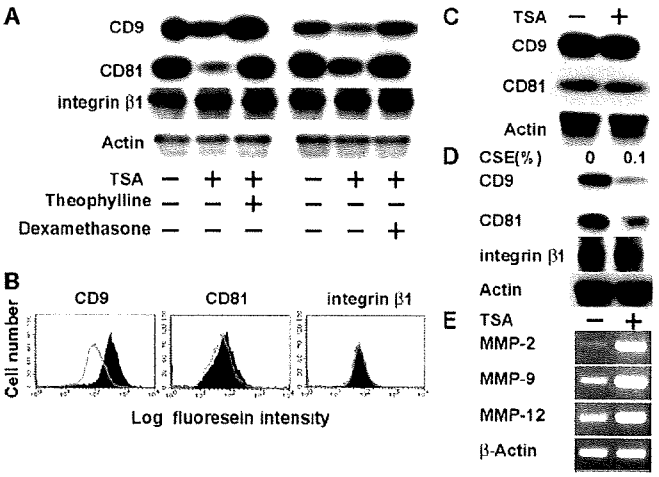

FIGURE 1. **TSA or CSE down-regulates CD9 and CD81 while up-regulating MMPs in RAW264.7 macrophages.** *A*, RAW264.7 cells were cultured in the absence or presence of TSA, theophylline, and dexamethasone for 48 h. Expressions of CD9, CD81, and integrin β1 were examined by immunoblotting using whole cell lysates. Anti-actin blots confirm equal amounts of protein loaded in each lane. *B*, RAW264.7 was cultured in the absence (*filled histograms*) or presence (*open histograms*) of TSA. Surface expressions of CD9, CD81, and integrin β1 were analyzed by flow cytometry. *C*, A549 alveolar epithelial cells were cultured in the absence or presence of TSA. CD9 and CD81 were immunoblotted. *D*, RAW264.7 was cultured in the absence or presence of 0.1% CSE for 48 h. CD9, CD81, and integrin β1 were immunoblotted. *E*, RAW264.7 was cultured in the absence or presence of TSA. Expressions of MMP-2, MMP-9, and MMP-12 were analyzed by RT-PCR. β-Actin amplification was internal control.

Peripheral Quantitative Computed Tomography (pQCT) Analysis—Femurs were fixed with 10% buffered formalin and measured using an XCT Research SA (Stratec Medizintechnik, Pforzheim, Germany) as described previously (15). The contour of the total bone was determined automatically with the pQCT software algorithm. The cortical and trabecular parameters were obtained at the diaphysis and 2 mm from distal epiphysis, respectively. The total mineral content and strength strain index were determined as described previously (16).

RESULTS

CD9 and CD81 Are Down-regulated by Smoking-related Inflammatory Stimuli in RAW264.7 Macrophages—Cigarette smoke reduces the expression and activity of HDACs in macrophages of COPD patients, resulting in amplification of pro-inflammatory gene transcription (5). To examine the effect of lowered HDAC activities on CD9 and CD81 expression, RAW264.7 macrophages were cultured in the presence of a HDAC inhibitor, TSA. As shown in Fig. 1*A*, treatment of RAW264.7 with TSA induced a decrease in protein levels of CD9 and CD81. The effects were reversed by the addition of a low concentration of HDAC activators, theophylline and dexamethasone (17), suggesting that their down-regulation was specific to HDAC inactivation and not because of nonspecific cytotoxicity of 10 ng/ml TSA. As a control, we tested the expression of integrin β1 but found no change in the presence of these agents (Fig. 1*A*). Consistent with the immunoblotting data, flow cytometry showed that TSA decreases surface expressions of CD9 and, to a lesser extent, CD81 while not affecting integrin β1 (Fig. 1*B*). The inhibitory effect of TSA was not observed in an alveolar epithelial cell line, A549 (Fig. 1*C*). We also examined the effect of IFN-γ and TNF-α, which are pro-inflammatory cytokines elevated in smoke-induced inflammation (18), on RAW264.7. As shown in supplemental Fig. 1, although TNF-α had no effect, IFN-γ dose-dependently suppressed the expressions of CD9 and CD81. Finally, we directly treated RAW264.7 cells with CSE (10) and observed that 0.1% CSE similarly reduced CD9 and CD81 but not integrin β1 in immunoblotting (Fig. 1*D*) and flow cytometry (data not shown). These results suggest that cigarette smoke may induce macrophages to down-regulate CD9 and CD81 expression in a cell-autonomous manner.

MMP production of macrophages is an essential part of pathophysiological mechanisms of COPD (1, 2). To examine the effect of HDAC inactivation, expressions of MMP-2, MMP-9, and MMP-12 were analyzed by RT-PCR. As shown in Fig. 1*E*, these MMPs were up-regulated with the addition of TSA. Based on these results, we hypothesized that the decrease of CD9 and CD81 may be upstream events to the increase of MMPs in macrophages stimulated with cigarette smoke.

mAbs or siRNA Transfection against CD9 and CD81 Enhance MMP Production and Suppress Cell Motility of RAW264.7—To examine if the loss of CD9 and CD81 function is causal to the up-regulation of MMPs, we treated RAW264.7 with function-inhibitory mAbs (13). Co-addition of anti-CD9 mAb, KMC8, and anti-CD81 mAb, 2F7, to RAW264.7 promoted the transcription of MMP-2 and MMP-9, although MMP-12 was unchanged (Fig. 2*A*). Up-regulation of TIMP-1 was also observed; this might be a counteraction against overproduction of MMP-9 (19). In gelatin zymography using culture supernatant, the addition of KMC8 or 2F7 increased gelatinolytic activity of MMP-9 compared with control, and the combination of KMC8 and 2F7 had an additive effect, suggesting a coordinate role of CD9 and CD81 in MMP-9 production (Fig. 2*B*). We failed to detect MMP-2 activity (data not shown) despite its transcription (Fig. 2*A*), possibly because of its defective activation in this cell line (20). MMP-9 activity was also examined by knockdown of CD9 or CD81 with siRNA transfection. As shown in Fig. 2*C*, protein levels of CD9 or CD81 were successfully lowered relative to control, and MMP-9 activity was increased by 75 and 49% in densitometry, respectively.

One of major tetraspanin functions is to regulate cell motility by forming complexes with integrins (21). In fact, we previously demonstrated that CD9 and CD81 complex with β1 and β2 integrins in blood monocytes (13). To study effects of the anti-tetraspanin mAbs on RAW264.7 motility, a migration assay was performed using Transwells (Fig. 2*D*). Although these mAbs did not affect cell proliferation and adhesion (data not shown), KMC8 and 2F7 suppressed migration of RAW264.7 cells on FN. Co-addition of anti-CD9 and anti-CD81 mAbs revealed an additive effect. The migration was dependent on β1 integrins because it was almost completely blocked by anti-integrin β1 mAb. Thus, CD9 and CD81 appeared to regulate integrin-dependent motility as well as MMP production in RAW264.7 macrophages.

CD9/CD81 DKO Mice Spontaneously Develop Pulmonary Emphysema—CD9/CD81 DKO mice were generated in our previous work, which reported that the fusion of mononuclear phagocytes were accelerated in these mice (13). Remarkably, we

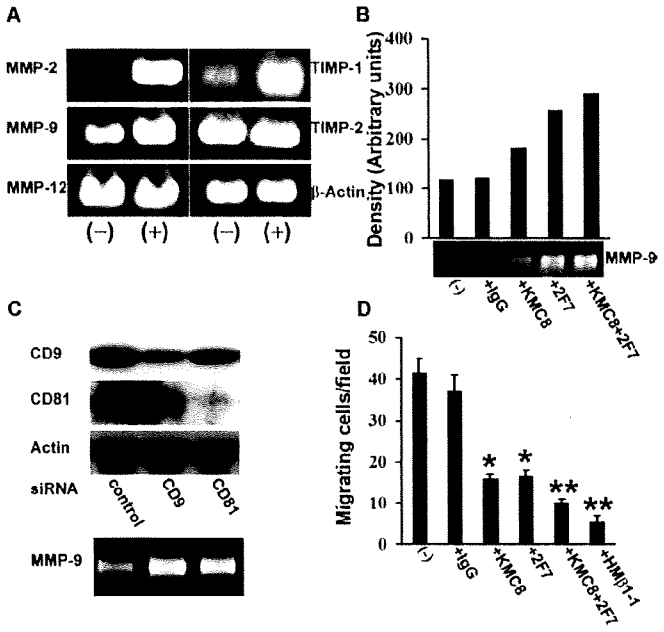

FIGURE 2. **mAbs or siRNA to CD9 and CD81 enhance MMP production and suppress motility of RAW264.7 cells.** *A*, RAW264.7 cells were cultured for 24 h in the absence (−) or presence of KMC8 plus 2F7 (+). mRNA was extracted, and RT-PCR was performed for expressions of MMPs and TIMPs. *B*, RAW264.7 cells were cultured for 24 h in the absence (−) or presence of the indicated mAbs. MMP-9 activity in culture supernatant was examined by gelatin zymography (*lower*) and quantified by densitometry (*upper*). The gelatin zymography is from one representative of three similar experiments. *C*, RAW264.7 was transfected with siRNAs against CD9 or CD81. Decrease in CD9 or CD81 was shown in immunoblotting (*upper*). MMP-9 activity in supernatants of 24-hour culture was examined by gelatin zymography (*lower*). *D*, RAW264.7 cells were applied into the upper chamber of FN-precoated Transwells in the absence (−) or presence of the indicated mAbs. DMEM containing 10% FBS was added to the lower chamber. After 4 h, cells migrating to the lower surface of the membrane were counted after Diff-Quick stain. *Bars* represent the mean ± S.E. *, $p < 0.05$ *versus* IgG; **, $p < 0.05$ *versus* KMC8. *KMC8*, anti-CD9; *2F7*, anti-CD81; *HMβ1-1*, anti-integrin β1.

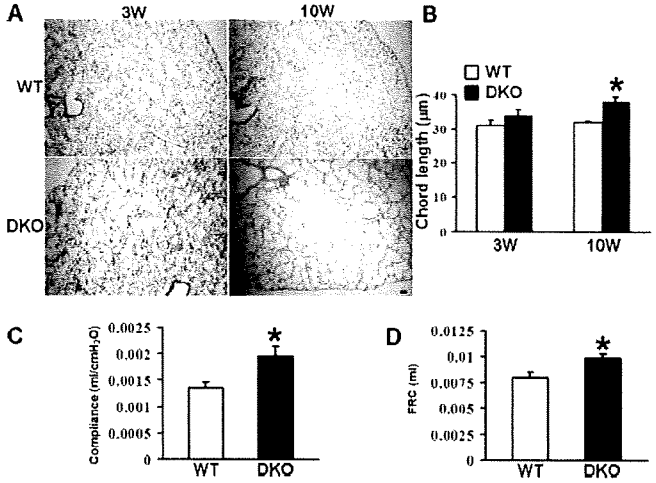

FIGURE 3. **CD9/CD81 DKO mice develop pulmonary emphysema.** *A*, histological lung sections from DKO mice and WT littermates at 3 and 10 weeks of age were stained with hematoxylin and eosin. *Bar*, 50 μm. *B*, chord length measured from the WT and DKO lungs. *C* and *D*, functional tests of the lung. Lung compliance (*C*) and functional residual capacity (*FRC*) (*D*) of mice at 23 weeks of age were measured with a whole body plethysmograph. Values were normalized to body weight. At least three mice were used for each group. *Bars* represent the mean ± S.E. *, $p < 0.05$ *versus* WT.

also found that the DKO mice developed pulmonary emphysema; the mutant lung showed enlargement of airspace and infiltration of inflammatory cells with age (Fig. 3, *A* and *B*, and supplemental Fig. 2). As shown in chord length measurement, the airspace size of CD9/CD81 DKO mice was not different from wild-type (WT) littermates at 3 weeks of age but significantly increased at 10 weeks (Fig. 3*B*). CD9 and CD81 single-KO mice also displayed mild focal airspace enlargement in close examination (supplemental Fig. 2*A*), but their chord lengths at 10 weeks were not significantly different from WT (data not shown). We next assessed the DKO lung using a whole body plethysmograph. When compared with the WT lung, static compliance (Fig. 3*C*) and functional residual capacity (Fig. 3*D*) were significantly increased, indicating physiological impairment of lung function.

It is believed that elastin degradation and remodeling processes occur within human emphysematous lungs (22). To investigate the pathogenesis of the emphysema of DKO lungs in more detail, we did additional staining and ultrastructural studies of histological sections. As shown in Fig. 4, *A* and *B*, elastin fibers appeared to be disrupted, and their network was lost in Elastica-van Gieson stain. Masson's trichrome stain of the enlarged alveolar region revealed abnormal deposition of collagen, suggesting the occurrence of a repair process (Fig. 4, *C* and *D*) (23). Of note, in the terminal bronchiole, Alcian blue/PAS stain detected secretory cell metaplasia of the epithelium (Fig. 4*F*), a finding not present in the WT bronchiole (Fig. 4*E*). In electron microscopy, alveolar macrophages developed many lysosomes and vacuoles (Fig. 4*G*). Some were multinucleated and contained intracytoplasmic needle-shaped inclusions (Fig. 4*H*), which appeared to be phagocytosed collagen as shown previously in destructive process of animal models of emphysema (24). These changes were again not observed in WT macrophages (Fig. 4*I*). There were also abnormal findings in the alveolar septa of the DKO lung. Type II epithelial cells were hypertrophic and contained many lamellar bodies (Fig. 4*J*). Localized increase of elastin and collagen fibers in alveolar walls (Fig. 4*K*), presumably representing structural remodeling (22), was noted when compared with WT (Fig. 4*L*). Collectively, these finding suggest that alveolar destruction and remodeling process were ongoing in the emphysematous lung of DKO mice.

It was previously proposed that apoptosis of septal epithelial and endothelial cells is part of the pathogenesis of emphysema (25). To examine if cell apoptosis contributes to emphysema of the DKO lung, lung sections were stained by terminal deoxynucleotidyltransferase-mediated dUTP nick-end labeling (supplemental Fig. 3*A*), and immunoblotting for active caspase-3 was done using whole lung lysates (supplemental Fig. 3*B*). However, no increase of apoptosis was observed in the DKO lung. We additionally induced apoptosis of bone marrow-derived macrophages (BMDMs) isolated from WT and DKO mice by depriving FBS in culture, but detected no significant difference (supplemental Fig. 3*C*).

Accumulation of Macrophages and Elevation of MMP Activities in the Lung of DKO Mice—Inflammation and protease overactivity are essential causal factors for emphysema lungs in humans (2). To examine if the double deletion of CD9 and CD81 leads to these pathogenic conditions *in vivo*, inflamma-

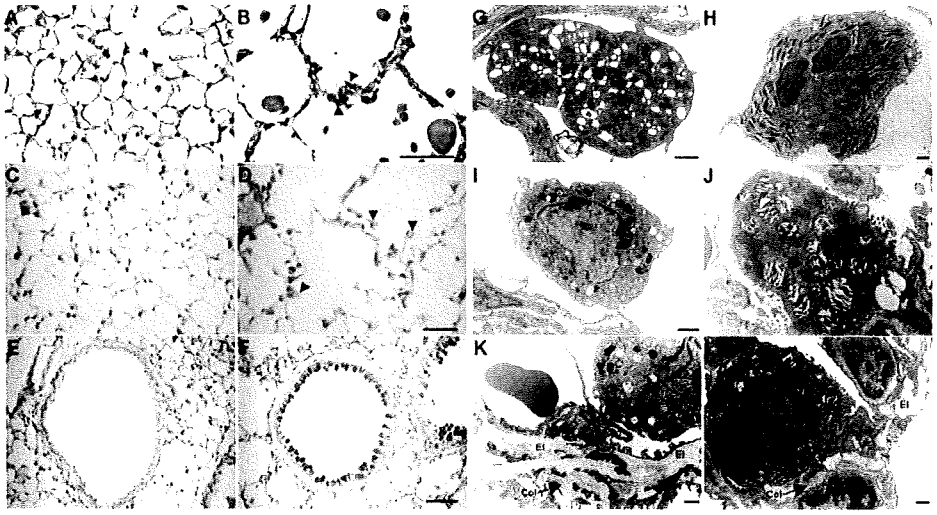

FIGURE 4. **Histological lung sections from DKO mice and WT littermates.** *A–F*, Elastica-van Gieson stain for elastin (*dark blue*) (*A* and *B*), Masson's trichrome stain for collagen (*blue*) (*C* and *D*), and Alcian blue/PAS stain (*E* and *F*) of lung sections from WT (*A*, *C*, and *E*) and DKO (*B*, *D*, and *F*) mice at 10 weeks of age. *Arrowheads* in *B* and *D* indicate sparse elastin fibers and abnormal deposition of collagen, respectively. *Bars*, 50 μm. *G–L*, a macrophage with many lysosomes and vacuoles (*G*), a macrophage containing needle-shaped inclusions (*H*), a hypertrophic type II cells accumulating lamellar bodies (*J*), and increased elastin and collagen fibers (*K*), were shown in electron microscopy of an alveolar region of DKO mice. A macrophage (*I*) and elastin and collagen (*L*) in an alveolar region of a WT littermate were also shown as control. *El*, elastin; *Col*, collagen. *Bars*, 1 μm.

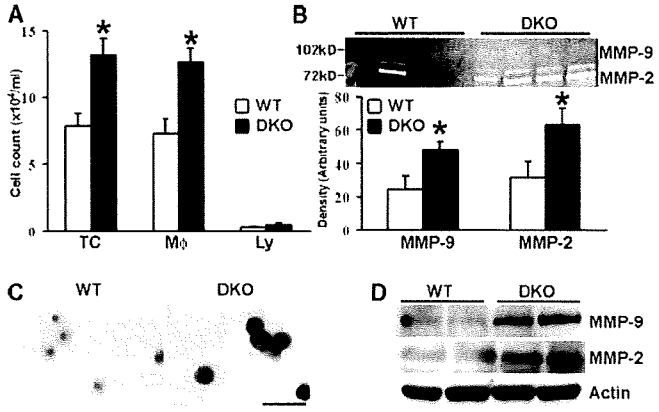

FIGURE 5. **Accumulation of macrophages and elevation of MMP activities in the DKO lung.** *A*, cells isolated from BALF of DKO mice and WT littermates at 10 weeks of age were visualized using Diff-Quick stain, and the number of total cells (*TC*), macrophages (*Mϕ*), and lymphocytes (*Ly*) was determined. *B*, MMP activities in BALF from individuals of DKO mice and WT littermates were examined by gelatin zymography (*upper*) and quantified by densitometry (*lower*). *Bars* represent the mean ± S.E. *, $p < 0.05$ *versus* WT. *C*, macrophages from the BALF were stained with anti-MMP-9 antibody. *Bar*, 100 μm. *D*, expressions of MMP-2 and MMP-9 were examined by immunoblotting using lung homogenate protein from individuals of WT and DKO mice. Anti-actin blots confirm equal amounts of protein loaded in each lane.

tory cells and MMP activities in the DKO lung were evaluated by BALF analysis. As shown in Fig. 5*A*, a larger number of inflammatory cells were isolated from the DKO lung than from WT, and this was because of an increase of macrophages. BALF from CD9 and CD81 single-KO mice contained slightly increased numbers of cells, but they were not significantly different from WT (supplemental Fig. 2*B*). Gelatin zymography showed that the BALF supernatants from DKO mice contained increased proteolytic activities of MMP-2 and MMP-9 (Fig. 5*B*). Also, macrophages isolated from the BALF were strongly stained with anti-MMP-9 antibody especially at the cell periphery, when compared with WT macrophages (Fig. 5*C*). We failed to detect obvious difference in the staining with anti-MMP-2 antibody (data not shown). Increase of the MMP proteins was also confirmed in lysates of the entire lung of DKO mice (Fig. 5*D*).

Macrophages from DKO Mice Are Less Motile and Produce More MMPs than WT—To confirm that motility and MMP production of macrophages in CD9/CD81 DKO mice are intrinsically altered like mAb- or siRNA-treated RAW264.7 cells (Fig. 2), we isolated and cultured BMDMs from DKO mice and compared with WT macrophages *in vitro*. Cell proliferation or cell adhesion onto FN or Matrigel was not different as shown in Fig. 6, *A* and *B*, respectively. However, when migration and random motility were examined in assays using Transwells (Fig. 6*C*) and a time-lapse video microscope (Fig. 6*D* and supplemental video 1), respectively (26), those of DKO macrophages were markedly decreased compared with WT cells. Also, expressions of MMP-2 and MMP-9, but not that of MMP-12, were increased (Fig. 6*E*), similarly to mAb- or siRNA-treated RAW264.7 cells. As a control, we isolated lung fibroblasts from WT and DKO mice and examined MMP-2 and MMP-9 production in gelatin zymography, but we found no differences (data not shown).

Analysis of Gene Expression in CD9/CD81 DKO Macrophages—To gain further information on altered macrophage function of DKO mice, we compared gene expression profiles of BMDMs isolated from WT and DKO mice with oligonucleotide arrays consisting of more than 20,000 mouse genes. The supplemental Tables 1 and 2 list the top 70 genes up-regulated or down-regulated preferentially in the DKO macrophages, respectively. Interestingly, fold differences of the down-regulated genes were higher than those of the up-regulated, also indicating that suppressed genes were much more than induced genes. The induced genes included proteases (carboxypeptidase A5; cathepsin E; cathepsin H; MMP-9; arginyl aminopeptidase (aminopeptidase B)), adhesion-related proteins (cortactin; syndecan 1; glypican 1; integrin αX), and pro-inflammatory cytokine receptors (CD74 (macrophage migration inhibitory factor receptor); colony-stimulating factor 2 receptor). Meanwhile, the suppressed genes included an antioxidant protein (ceruloplasmin), a protease inhibitor (serine peptidase inhibitor, clade B, members 5 (Maspin)), and extracellular matrix proteins (integrin-binding sialoprotein; secreted acidic cysteine-rich glycoprotein (osteonectin); biglycan; matrilin 3). It is of note that fucosyltransferase 8 was listed as a down-regulated gene in the DKO macrophages, because the deficiency of this glycosyltransferase was recently reported to impair $\alpha 3\beta 1$ inte-

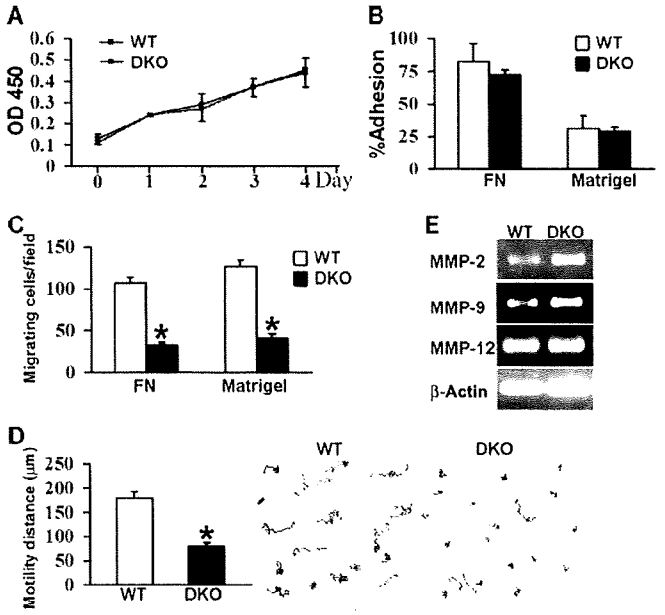

FIGURE 6. **BMDMs from DKO mice are less motile and produce more MMPs than WT.** *A*, BMDMs from DKO mice or WT littermates at 10 weeks of age were cultured in DMEM containing 20% FBS and 30% L929 supernatant. Cell proliferation was quantified using Cell Counting Kit-8. *B*, BMDMs in serum-free DMEM were cultured on FN- or Matrigel-precoated wells for 1.5 h. After unattached cells were removed, adherent cells were quantified with Cell Counting Kit-8. *C*, BMDMs in serum-free DMEM were applied to the upper chamber of Transwells that were precoated with FN or Matrigel. DMEM containing 10% FBS was added to the lower chamber. After 4 h, cells migrating to the lower surface were counted with Diff-Quick stain. *D*, BMDMs were plated onto Matrigel-precoated dishes. Images were acquired every minute for 90 min, and tracks (*right*) and distances (*left*) of random motility were determined using Scion Image tools. Values represent the mean ± S.E. *, $p < 0.05$ *versus* WT. *E*, mRNA was extracted from BMDMs, and expressions of MMP-2, MMP-9, and MMP-12 were analyzed by RT-PCR. β-Actin amplification was internal control.

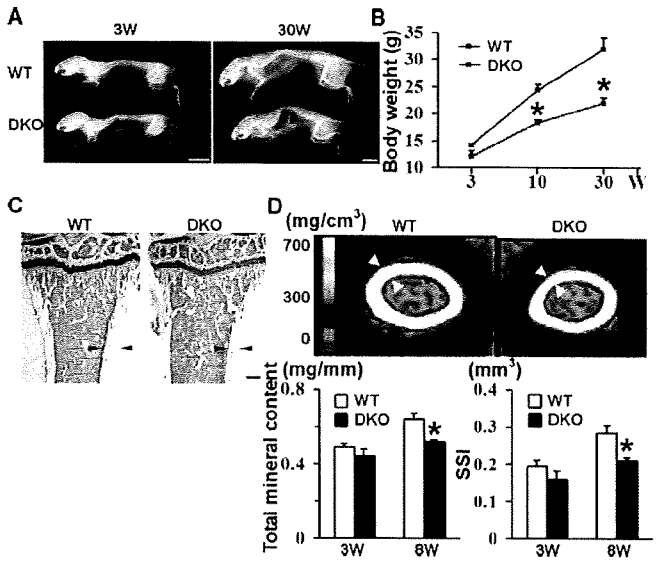

FIGURE 7. **CD9/CD81 DKO mice display body weight loss, kyphosis, and osteopenia.** *A*, whole body radiographs of WT and DKO mice at 3 and 30 weeks of age. *Bars*, 10 mm. *B*, time course of body weight of WT and DKO littermates. *C*, toluidine blue stain of longitudinal sections of proximal tibia at 8 weeks of age. Note that cortical bone of the DKO mouse is thinner than that of the WT littermate (*arrowheads*). *Bar*, 250 μm. *D*, pQCT images of femoral diaphysis at 8 weeks of age (*upper*). Mineral densities are shown as different colors according to the standard mineral density gradients. Note the reduction in cortical thickness of the DKO mouse (*arrowheads*). Total mineral content and strength strain index (*SSI*) were also determined (*lower*). Trabecular parameters were not different between WT and DKO mice (data not shown). Values represent the mean ± S.E. *, $p < 0.05$ *versus* WT.

grin-mediated cell migration and cause pulmonary emphysema in mice (27). Expressions of other tetraspanins, including CD37, CD53, CD82, and CD151, were unremarkably changed (data not shown).

CD9/CD81 DKO Mice Also Display Body Weight Loss, Kyphosis, and Osteopenia—With aging, the DKO mice could be discriminated from WT (Fig. 7*A*) and CD9 or CD81 single-KO littermates (data not shown) by progressive kyphotic appearance, as shown in whole body radiographs. Moreover, weight loss became evident over time when compared with WT mice (Fig. 7*B*). Histological sections of proximal tibia displayed that, although the trabecular bone appeared normal, the cortical bone of DKO mice was thinner than WT (Fig. 7*C*). Images of femoral diaphysis in pQCT analysis also showed a decrease in cortical bone thickness and age-dependent reduction in total mineral content and strength strain index (Fig. 7*D*). Decrease in these parameters was not observed in CD9 or CD81 single-KO mice (data not shown). To investigate the pathophysiology of the osteopenic phenotype in more detail, histomorphometric analysis was done with the proximal tibia of DKO mice (supplemental Fig. 4). Consistently with the histological appearance of the trabecular bone (Fig. 7*C*), there were no significant differences in trabecular bone volume and trabecular thickness (supplemental Fig. 4*A*). The number of osteoclasts in the DKO mice was increased by 60% when compared with WT (supplemental Fig. 4*B*). This seems to reflect elevated fusogenic capacity of DKO macrophages *in vitro* (supplemental Fig. 4*C*) and is consistent with our previous observation (13). However, eroded surface was decreased (supplemental Fig. 4*B*), suggesting that osteoclast activity was unexpectedly impaired. Meanwhile, osteoblast activity was likewise reduced. The number of osteoblasts and the surface of osteoblasts were decreased, and their function in matrix production was damaged as indicated by the decreased thickness of newly deposited matrix (osteoid thickness) (supplemental Fig. 4, *D* and *E*). To perform kinetic analysis of bone formation and mineralization, mice were intraperitoneally injected twice with calcein at a 3-day interval. Compared with WT, the distance of two labeled bands was shorter in the DKO mice (supplemental Fig. 4*F*), resulting in decreased mineral apposition rate and bone formation rate in trabecular dynamic histomorphometry (supplemental Fig. 4*G*). These results indicate that, although osteoclastogenesis is accelerated, both osteolytic and osteoblastic activities were impaired and that the decrease of bone formation rather exceeded that of bone resorption.

We further analyzed histological sections of muscle, skin, eye, heart, aorta, liver, and kidney, but no obvious difference was observed between WT and DKO mice. Hemoglobin and the number of leukocytes and platelets determined in peripheral blood analysis were normal. Serum levels of total protein, albumin, cholesterol, triglyceride, calcium, and creatinine were also not different (data not shown). Thus, the phenotype is unlikely to be caused by malnutrition, and the CD9/CD81 DKO

mouse is not a premature aging model such as *klotho* mice, which exhibits ectopic calcifications, arteriosclerosis, skin atrophy, and cardiac dysfunction in addition to pulmonary emphysema and osteopenia (28).

DISCUSSION

At specialized membrane microdomains, tetraspanins facilitate the formation of multimolecular complexes and regulate cell morphology, motility, invasion, fusion, and signaling. Based on these characteristics, they are also referred to as molecular facilitator or organizer (6). Tetraspanins have been extensively studied in cancer biology. They affect tumor cell motility *in vitro* and tumor metastasis *in vivo* most likely by regulating function of integrins and production of MMPs (7–9, 29). However, it has not been investigated if tetraspanins play a role in motility and MMP production of macrophages. Using a mAb- or siRNA-treated macrophage line, RAW264.7 (Fig. 2), and primary DKO macrophages (Fig. 6), we have shown that dysfunction of CD9 and CD81 suppresses cell motility and promoted the production of MMP-2 and MMP-9 *in vitro*. CD9/CD81 double deletion also caused increase of macrophages and elevation of MMP-2 and MMP-9 activities in the mouse lung *in vivo* (Fig. 5). Thus, co-deficiency of CD9 and CD81 function seems to be sufficient for macrophages to increase MMP production as well as to suppress cell motility. Suppressed motility of macrophages does not necessarily contradict with their infiltration into the lung. For example, macrophages from SH2-containing inositol-5-phosphatase 1 (SHIP1) KO mice, which revealed massive infiltration of macrophages in alveolar air spaces, exhibited defects in motility *in vitro* (30). In these mice, decreased efflux of macrophages from the airspace, rather than their increased influx into the airspace, might contribute to macrophage accumulation. The expression of MMPs is regulated by multiple factors, including growth factors and their receptors, cell adhesion molecules, and GTPases (31). We speculate that CD9 and CD81 coordinately assemble these factors in their own microdomains and thereby indirectly control the production of MMPs (6).

Expression of inflammatory genes is determined by a balance between histone acetylation, which activates transcription, and deacetylation, which switches off transcription. In humans, cigarette smoke suppresses the activity of HDAC in alveolar macrophages, and this was correlated with increased expression of inflammatory genes, including TNF-α and IL-8 in these cells. There was also a reduction in HDAC activity in peripheral lung and alveolar macrophages from COPD patients, and this was correlated with disease severity (5). We cultured RAW264.7 cells in the presence of CSE, the HDAC inhibitor TSA, and pro-inflammatory cytokines IFN-γ and TNF-α, and all these treatments but TNF-α down-regulated the protein levels of both CD9 and CD81 (Fig. 1 and supplemental Fig. 1). These results raise an hypothesis that cigarette smoke reduces the HDAC activity, switching on inflammatory genes and leading to the down-regulation of CD9 and CD81 in macrophages. The resultant insufficiency of CD9 and CD81 functions may be part of important mechanisms that cause or exacerbate the accumulation of alveolar macrophages and their overproduction of MMPs in cigarette smokers.

CD9 single-KO mice are infertile because of impaired oocyte fusion with sperm (32). CD81 single-KO mice show likewise impaired oocyte fertilization (33) in addition to altered immune response (34, 35). KO mice of single tetraspanin have so far resulted in relatively mild phenotype. One possible reason is that the loss of a single tetraspanin may be compensated by other tetraspanins (21). In this study, double deletion of CD9 and CD81 in mice leads to the lung phenotype morphologically and functionally mimicking the emphysematous lung in human COPD (Fig. 3). The CD9/CD81 DKO mice displayed age-dependent progression of airspace enlargement. Secretory cell metaplasia, a finding similar to goblet cell metaplasia in cigarette smokers (36), was also observed. It is unlikely that the emphysema resulted from defective alveolization, because mouse alveolization is completed by 3 weeks (37). Moreover, the elastin/collagen staining and ultrastructural studies of histological sections suggested that alveolar destruction and remodeling process were ongoing in the DKO lung (Fig. 4). Thus, together with the findings of macrophage infiltration and elevated MMP activities in the lung (Fig. 5), it appears that inflammatory and elastolytic processes caused emphysema in the DKO mice. In the gene expression profile of DKO macrophages, multiple proteases, including MMP-9, were induced (supplemental Table 1), whereas the antioxidant protein ceruloplasmin, the protease inhibitor Maspin, and multiple extracellular matrix proteins were suppressed (supplemental Table 2). Although these differential gene expressions remain to be validated with quantitative PCR, the profile was consistent with the hypothesis that the imbalances of proteases/antiproteases and oxidants/antioxidants were present in the DKO macrophages as proposed previously for molecular mechanisms in macrophages orchestrating the progression of emphysema (2).

Common extrapulmonary effects of COPD include weight loss and osteoporosis, mechanisms of which have been poorly understood (38, 39). Interestingly, the CD9/CD81 DKO mice displayed age-dependent weight loss and osteopenia (Fig. 7). The number of osteoclasts was increased because of the enhanced fusion of their progenitors of the macrophage lineage, but the osteopenia was caused not by increased bone resorption but by decreased bone formation (supplemental Fig. 4), indicating low turnover osteopenia. This type of osteopenia occurs as an aging process in humans (40), and it has been proposed that there are clear parallels between the pathophysiological responses to aging and those involved in COPD (41). To assess the function of the DKO osteoblasts *in vitro*, we isolated and cultured bone marrow cells in the presence of ascorbic acid and β-glycerophosphate and stained mineralized nodules with alizarin red (42). However, preliminary results failed to reveal obvious differences between WT and DKO mice (data not shown). Possibly, the impaired bone formation in DKO mice might be attributed not to primary defects of osteoblasts but to their microenvironmental factors such as hormones, cytokines, growth factors, MMPs, and extracellular matrix proteins

(43, 44). Dysfunction of other cell lineage may also be indirectly involved in impaired osteoblast function *in vivo*. For example, the defective production of osteonectin and biglycan in bone marrow macrophages, as shown in our gene expression analysis (supplemental Table 2), might damage osteoblast functions in the DKO mice as described previously (45, 46).

Cigarette smoking is known as a common risk factor for COPD and osteoporosis, which are both characterized by net loss of lung or bone tissue mass (47), and the phenotype of DKO mice has raised a possibility that these two pathological conditions might share common mechanisms involving tetraspanins. Further studies using human samples are needed because there are considerable differences in physiology and anatomy between mice and humans (48).

In conclusion, this study has shown that tetraspanins CD9 and CD81, which regulate motility and MMP production of macrophages, are down-regulated by smoking-related pro-inflammatory stimuli. Double deficiency of these tetraspanins causes age-related progression of pulmonary emphysema and osteopenia in mice. Given that tetraspanins function as molecular facilitator, the loss of CD9 and CD81 could lead to disordered organization of molecules that otherwise associate with these tetraspanins. Such defective molecular organization might be a part of mechanisms underlying the lung disease and osteoporosis in human COPD.

Acknowledgments—We thank T. Miyazaki (University of Texas Southwestern Medical Center, Dallas) for providing CD81 KO mice; M. Kobayashi (Osaka University) for assistance in mouse genotyping; Y. Tomita and S. Furue (Shionogi and Co., Ltd., Osaka, Japan) for assistance in chord length measurement; T. Yoneda (Osaka University Graduate School of Dentistry, Osaka, Japan) for helpful comments on bone analysis; T. Ito and K. Ozawa (Osaka University Graduate School of Medicine) for helpful comments on kidney and skin histology, respectively; Y. Satou (Teijin Pharma Ltd.) and M. Hamaoka (Osaka University) for technical assistance; and Y. Habe for secretarial assistance.

REFERENCES

1. Shapiro, S. D. (2002) *Biochem. Soc. Trans.* **30,** 98–102
2. Barnes, P. J., Shapiro, S. D., and Pauwels, R. A. (2003) *Eur. Respir. J.* **22,** 672–688
3. Finlay, G. A., O'Driscoll, L. R., Russell, K. J., D'Arcy, E. M., Masterson, J. B., FitzGerald, M. X., and O'Connor, C. M. (1997) *Am. J. Respir. Crit. Care Med.* **156,** 240–247
4. Ohnishi, K., Takagi, M., Kurokawa, Y., Satomi, S., and Konttinen, Y. T. (1998) *Lab. Investig.* **78,** 1077–1087
5. Barnes, P. J. (2006) *Chest* **129,** 151–155
6. Hemler, M. E. (2005) *Nat. Rev. Mol. Cell Biol.* **6,** 801–811
7. Sugiura, T., and Berditchevski, F. (1999) *J. Cell Biol.* **146,** 1375–1389
8. Saito, Y., Tachibana, I., Takeda, Y., Yamane, H., He, P., Suzuki, M., Minami, S., Kijima, T., Yoshida, M., Kumagai, T., Osaki, T., and Kawase, I. (2006) *Cancer Res.* **66,** 9557–9565
9. Tohami, T., Drucker, L., Shapiro, H., Radnay, J., and Lishner, M. (2007) *FASEB J.* **21,** 691–699
10. Hoshino, S., Yoshida, M., Inoue, K., Yano, Y., Yanagita, M., Mawatari, H., Yamane, H., Kijima, T., Kumagai, T., Osaki, T., Tachiba, I., and Kawase, I. (2005) *Biochem. Biophys. Res. Commun.* **329,** 58–63
11. Shibata, Y., Zsengeller, Z., Otake, K., Palaniyar, N., and Trapnell, B. C. (2001) *Blood* **98,** 2845–2852
12. Wang, Z., Zheng, T., Zhu, Z., Homer, R. J., Riese, R. J., Chapman, H. A., Jr., Shapiro, S. D., and Elias, J. A. (2000) *J. Exp. Med.* **192,** 1587–1600
13. Takeda, Y., Tachibana, I., Miyado, K., Kobayashi, M., Miyazaki, T., Funakoshi, T., Kimura, H., Yamane, H., Saito, Y., Goto, H., Yoneda, T., Yoshida, M., Kumagai, T., Osaki, T., Hayashi, S., Kawase, I., and Mekada, E. (2003) *J. Cell Biol.* **161,** 945–956
14. Zheng, T., Zhu, Z., Wang, Z., Homer, R. J., Ma, B., Riese, R. J., Jr., Chapman, H. A., Jr., Shapiro, S. D., and Elias, J. A. (2000) *J. Clin. Investig.* **106,** 1081–1093
15. Liu, W., Toyosawa, S., Furuichi, T., Kanatani, N., Yoshida, C., Liu, Y., Himeno, M., Narai, S., Yamaguchi, A., and Komori, T. (2001) *J. Cell Biol.* **155,** 157–166
16. Lind, P. M., Lind, L., Larsson, S., and Orberg, J. (2001) *Bone (Elmsford)* **29,** 265–270
17. Ito, K., Lim, S., Caramori, G., Cosio, B., Chung, K. F., Adcock, I. M., and Barnes, P. J. (2002) *Proc. Natl. Acad. Sci. U. S. A.* **99,** 8921–8926
18. Park, G. Y., Park, J. W., Jeong, D. H., and Jeong, S. H. (2003) *Chest* **123,** 475–480
19. Cawston, T., Carrere, S., Catterall, J., Duggleby, R., Elliott, S., Shingleton, B., and Rowan, A. (2001) *Novartis Found. Symp.* **234,** 205–228
20. Ogawa, K., Chen, F., Kuang, C., and Chen, Y. (2004) *Biochem. J.* **381,** 413–422
21. Hemler, M. E. (2003) *Annu. Rev. Cell Dev. Biol.* **19,** 397–422
22. Finlay, G. A., O'Donnell, M. D., O'Connor, C. M., Hayes, J. P., and FitzGerald, M. X. (1996) *Am. J. Pathol.* **149,** 1405–1415
23. Jeffery, P. K. (2001) *Am. J. Respir. Crit. Care Med.* **164,** S28–S38
24. Lucattelli, M., Cavarra, E., de Santi, M. M., Tetley, T. D., Martorana, P. A., and Lungarella, G. (2003) *Eur. Respir. J.* **22,** 728–734
25. Kasahara, Y., Tuder, R. M., Cool, C. D., Lynch, D. A., Flores, S. C., and Voelkel, N. F. (2001) *Am. J. Respir. Crit. Care Med.* **163,** 737–744
26. Takeda, Y., Kazarov, A. R., Butterfield, C. E., Hopkins, B. D., Benjamin, L. E., Kaipainen, A., and Hemler, M. E. (2007) *Blood* **109,** 1524–1532
27. Wang, X., Inoue, S., Gu, J., Miyoshi, E., Noda, K., Li, W., Mizuno-Horikawa, Y., Nakano, M., Asahi, M., Takahashi, M., Uozumi, N., Ihara, S., Lee, S. H., Ikeda, Y., Yamaguchi, Y., Aze, Y., Tomiyama, Y., Fujii, J., Suzuki, K., Kondo, A., Shapiro, S. D., Lopez-Otin, C., Kuwaki, T., Okabe, M., Honke, K., and Taniguchi, N. (2005) *Proc. Natl. Acad. Sci. U. S. A.* **102,** 15791–15796
28. Nabeshima, Y. (2002) *Ageing Res. Rev.* **1,** 627–638
29. Chirco, R., Liu, X. W., Jung, K. K., and Kim, H. R. (2006) *Cancer Metastasis Rev.* **25,** 99–113
30. Nishio, M., Watanabe, K., Sasaki, J., Taya, C., Takasuga, S., Iizuka, R., Balla, T., Yamazaki, M., Watanabe, H., Itoh, R., Kuroda, S., Horie, Y., Forster, I., Mak, T. W., Yonekawa, H., Penninger, J. M., Kanaho, Y., Suzuki, A., and Sasaki, T. (2007) *Nat. Cell Biol.* **9,** 36–44
31. Greenlee, K. J., Werb, Z., and Kheradmand, F. (2007) *Physiol. Rev.* **87,** 69–98
32. Miyado, K., Yamada, G., Yamada, S., Hasuwa, H., Nakamura, Y., Ryu, F., Suzuki, K., Kosai, K., Inoue, K., Ogura, A., Okabe, M., and Mekada, E. (2000) *Science* **287,** 321–324
33. Rubinstein, E., Ziyyat, A., Prenant, M., Wrobel, E., Wolf, J. P., Levy, S., Le Naour, F., and Boucheix, C. (2006) *Dev. Biol.* **290,** 351–358
34. Maecker, H. T., and Levy, S. (1997) *J. Exp. Med.* **185,** 1505–1510
35. Miyazaki, T., Muller, U., and Campbell, K. S. (1997) *EMBO J.* **16,** 4217–4225
36. Wright, J. L., and Churg, A. (2002) *Chest* **122,** S301–S306
37. Amy, R. W., Bowes, D., Burri, P. H., Haines, J., and Thurlbeck, W. M. (1977) *J. Anat.* **124,** 131–151
38. Gross, N. J. (2001) *Curr. Opin. Pulm. Med.* **7,** 84–92
39. Agusti, A. (2007) *Proc. Am. Thorac. Soc.* **4,** 522–525
40. Manolagas, S. C., and Jilka, R. L. (1995) *N. Engl. J. Med.* **332,** 305–311
41. Tuder, R. M., Yoshida, T., Arap, W., Pasqualini, R., and Petrache, I. (2006) *Proc. Am. Thorac. Soc.* **3,** 503–510
42. Inoue, K., Mikuni-Takagaki, Y., Oikawa, K., Itoh, T., Inada, M., Noguchi, T., Park, J. S., Onodera, T., Krane, S. M., Noda, M., and Itohara, S. (2006) *J. Biol. Chem.* **281,** 33814–33824
43. Ortega, N., Behonick, D., Stickens, D., and Werb, Z. (2003) *Ann. N. Y. Acad. Sci.* **995,** 109–116

44. Hadjidakis, D. J., and Androulakis, I. I. (2006) *Ann. N. Y. Acad. Sci.* **1092,** 385–396
45. Xu, T., Bianco, P., Fisher, L. W., Longenecker, G., Smith, E., Goldstein, S., Bonadio, J., Boskey, A., Heegaard, A. M., Sommer, B., Satomura, K., Dominguez, P., Zhao, C., Kulkarni, A. B., Robey, P. G., and Young, M. F. (1998) *Nat. Genet.* **20,** 78–82
46. Delany, A. M., Amling, M., Priemel, M., Howe, C., Baron, R., and Canalis, E. (2000) *J. Clin. Investig.* **105,** 915–923
47. Agusti, A. G., Noguera, A., Sauleda, J., Sala, E., Pons, J., and Busquets, X. (2003) *Eur. Respir. J.* **21,** 347–360
48. Brusselle, G. G., Bracke, K. R., Maes, T., D'Hulst, A. I., Moerloose, K. B., Joos, G. F., and Pauwels, R. A. (2006) *Pulm. Pharmacol. Ther.* **19,** 155–165

MOLECULAR REPRODUCTION AND DEVELOPMENT 75:150–155 (2008)

Possible Involvement of CD81 in Acrosome Reaction of Sperm in Mice

MAYA TANIGAWA,[1,2] KIYOKO MIYAMOTO,[1] SATOSHI KOBAYASHI,[3] MASAHIRO SATO,[4] HIDENORI AKUTSU,[1] MASARU OKABE,[2,5] EISUKE MEKADA,[3] KEIICHI SAKAKIBARA,[1] MAMI MIYADO,[1] AKIHIRO UMEZAWA,[1] AND KENJI MIYADO[1,6,7]*

[1]*Department of Reproductive Biology and Pathology, National Center for Child Health and Development, Tokyo, Japan*
[2]*Faculty of Pharmaceutical Sciences, Osaka University, Osaka, Japan*
[3]*Research Institute for Microbial Diseases, Osaka University, Osaka, Japan*
[4]*Frontier Science Research Center, Kagoshima University, Kagoshima, Japan*
[5]*Genome Information Research Center, Osaka University, Osaka, Japan*
[6]*PREST, Japan Science and Technology Agency, Saitama, Japan*
[7]*School of Biomedical Science, Tokyo Medical and Dental University, Tokyo, Japan*

ABSTRACT Tetraspanin CD81 is closely homologous in amino acid sequence with CD9. CD9 is well known to be involved in sperm–egg fusion, and CD81 has also been reported to be involved in membrane fusion events. However, the function of CD81 as well as that of CD9 in membrane fusion remains unclear. Here, we report that disruption of the mouse CD81 gene led to a reduction in the fecundity of female mice, and CD81−/− eggs had impaired ability to fuse with sperm. Furthermore, we demonstrated that when CD81−/− eggs were incubated with sperm, some of the sperm that penetrated into the perivitelline space of CD81−/− eggs had not yet undergone the acrosome reaction, indicating that the impaired fusibility of CD81−/− eggs may be in part caused by failure of the acrosome reaction of sperm. In addition, we showed that CD81 was highly expressed in granulosa cells, somatic cells that surround oocytes. Our observations suggest that there is an interaction between sperm and CD81 on somatic cells surrounding eggs before the direct interaction of sperm and eggs. Our results may provide new clues for clarifying the cellular mechanism of the acrosome reaction, which is required for sperm–egg fusion. *Mol. Reprod. Dev. 75: 150–155, 2008.* © 2007 Wiley-Liss, Inc.

Key Words: CD9; acrosome reaction; fertilization; mice; zona pellucida

INTRODUCTION

Fertilization is accomplished by the direct interaction of sperm and eggs, a process mediated primarily by predicted, but yet unidentified gamete membrane proteins. In fertilization, the acrosome reaction is a change in sperm that is required for penetration into the zona pellucida, the egg coat, and facilitates the subsequent fusion with the egg plasma membrane (Moreno and Alvarado, 2006). Zona pellucida protein 3 (ZP3), one of the components forming the meshwork of the zona pellucida, has been considered to be the prime physiological inducer of the acrosome reaction in sperm, although the frequency of acrosome reaction is low after incubation with recombinant ZP3 (Beebe et al., 1992). This discrepancy suggests that, besides ZP3, unknown major factor(s) might be responsible for the acrosome reaction. To date, despite the importance of the acrosome reaction in fertilization, the underlying cellular mechanisms that regulate the acrosome reaction remain unclear.

Two tetraspanins, CD9 and CD81, are known to be important in the membrane fusion events in various biological systems. In virus-host cell fusion, human CD81 has been identified as a co-receptor for hepatitis C virus (Higginbottom et al., 2000; Cormier et al., 2004). Both CD9 and CD81 have been implicated in myoblast fusion (Tachibana and Hemler, 1999; Schwander et al., 2003) and monocyte/macrophage fusion in mice (Takeda et al., 2003). Recent studies using gene-targeting techniques demonstrated that female mice carrying a deletion of the CD9 gene produce eggs that mature normally but are defective in sperm–egg fusion (Kaji et al., 2000; Le Naour et al., 2000; Miyado et al., 2000; Takahashi et al., 2001). CD81 has also been reported to be expressed on the plasma membrane of unfertilized mouse eggs (Takahashi et al., 2001). Furthermore, CD81−/− mice have been reported to have defects in reproduction after several generations of backcrossing (Deng et al., 2000).

Grant sponsor: Precursory Research for Embryonic Science and Technology (PRESTO); Grant sponsor: The Ministry of Health, Labour and Welfare; Grant sponsor: The Ministry of Education, Culture, Sports, and Technology, of Japan.

*Correspondence to: Kenji Miyado, National Center for Child Health and Development, 2-10-1 Okura, Setagaya, Tokyo 157-8535, Japan. E-mail: kmiyado@nch.go.jp

Received 31 October 2006; Accepted 8 December 2006
Published online 8 February 2007 in Wiley InterScience (www.interscience.wiley.com).
DOI 10.1002/mrd.20709

Recently, Rubinstein et al. (2006) provided more detailed data showing that eggs of CD81−/− mice are unable to be fertilized with sperm, although the degree of the defect appeared not to be severe compared with that of CD9−/− eggs. Moreover, injection of CD9−/− eggs with mouse CD81 mRNA revealed that mouse CD81 was only moderately effective at reversing the infertility of CD9−/− eggs (Kaji et al., 2002). These findings taken together indicate that CD81 and CD9 each have different roles in fertilization.

Here we studied the role of CD81 in fertilization by in vitro fertilization (IVF) and immunohistochemical analysis, and propose a possible role of CD81 in the acrosome reaction in sperm.

MATERIALS AND METHODS

Animals

CD81−/− mice (Miyazaki et al., 1997) were kindly provided by Dr. Miyazaki and were backcrossed to C57BL/6 mice. Genotyping was carried out using polymerase chain reaction as previously described (Miyazaki et al., 1997). To visualize acrosome-intact sperm, EGFP-transgenic mice expressing EGFP in the acrosomes were generated by pronuclear injection of constructs carrying the EGFP gene driven by the mouse acrosin promoter (Nakanishi et al., 1999) and the DsRed2 gene tagged with a mitochondrial transport signal and driven by the CAG promoter into fertilized eggs of BDF1 mice (unpublished information). After the sperm were acrosome-reacted, EGFP was lost from the sperm heads and DsRed remained in the mitochondria of the mid-piece region. All animal procedures were performed according to protocols approved by the National Center for Child Health and Development and use committees.

Egg Collection

Female mice (aged 8–15 weeks) were injected with 5 U of hCG (Gonatropin; Aska Pharmaceutical Co., Ltd, Tokyo, Japan) 48 hr after administration of 5 U of PMSG (Serotropin; Aska Pharmaceutical Co., Ltd). Ovulated eggs were collected from the oviductal ampulla 13.5–15 hr after hCG injection, and placed in 100-μl drops of TYH medium equilibrated with 5% CO_2 in air at 37°C. Cumulus cells were removed with 300 IU/ml of hyaluronidase (H-3506, Sigma-Aldrich, Missouri, MO), and eggs were incubated with a defined number of sperm.

Sperm Preparation and In Vitro Fertilization

Sperm were collected by squeezing two cauda epididymides of 8- to 10-week-old B6C3F1 or transgenic male mice in a well containing 100-μl of TYH medium. Sperm were incubated at 37°C in 5% CO_2 for 90 min before being mixed with eggs derived from wild-type or CD81−/− female mice. The final concentration of sperm added to an egg-containing drop was 1.5×10^5 sperm/ml. To examine the rate of fertilization, we counted the number of eggs at the two-cell stage 24 hr after incubation with the sperm. For counting the number of fused sperm, the zona pellucida was removed from the eggs by a brief incubation in acid Tyrode solution, and sperm were incubated with eggs preloaded with 4′,6-diamidino-2-phenylindole (DAPI) for counting the number of sperm fused with eggs (Yamagata et al., 2002). For counting the number of acrosome-intact sperm, EGFP-expressing sperm were incubated with zona-intact CD81+/+ or CD81−/− eggs. The eggs were all subjected to confocal microscopic analysis for the presence of sperm exhibiting red and green fluorescence or red fluorescence alone within the perivitelline space 4 hr after incubation.

Immunostaining

For immunostaining of cryostat sections, ovaries from 8- to 10-week-old wild-type C57BL/6 females were fixed in 2% paraformaldehyde in PBS (−) for 2 days at 4°C, and then immersed in 30% sucrose in PBS (−) for more than 2 days at 4°C, embedded in Tissue-Tek OCT compound (Sakura Finetek Co., Tokyo, Japan), and finally frozen before serial cryostat sectioning (8 μm in thickness). Slides were fixed in an acetone and incubated with anti-CD81 antibody (Eat-1) diluted 1:300 in PBS (−) containing 0.1% bovine serum albumin (BSA), BSA/PBS (−), or anti-ZP3 antibody diluted 1:300 in BSA/PBS (−), overnight at 4°C. After washing three times with BSA/PBS (−), the samples were incubated with Alexa 546-conjugated goat anti-hamster IgG (A-21111, Invitrogen, California, CA) or Alexa 488-conjugated goat anti-rat IgG (A-11006, Invitrogen) for 2 hr at room temperature. After extensive washing, the slides were inspected for fluorescence using LSM 510 META confocal microscope.

Immunoblotting

Samples containing equal amounts of eggs were dissolved in nonreducing sample buffer and subjected to 12% SDS–PAGE according to procedures described previously (Miyado et al., 2000). After electrophoresis, the gels were transferred to PVDF membranes for immunoblot analysis. The blots were blocked in 1% nonfat dry milk, and were probed with the primary antibodies, anti-mouse CD81 antibody (Eat-1, BD Biosciences, California, CA) or anti-mouse CD9 antibody (KMC8, BD Biosciences). After washing in TBS-Tween buffer, the membranes were incubated with HRP-labeled secondary antibodies; goat anti-rat antibody or goat anti-hamster antibody. The expression level of immunoreacted products was determined by treatment of the blots with an ECL or ECL Plus Detection Kit (GE Healthcare Bio-Science Co., New Jersey, UK) and exposure to X-ray film at room temperature.

Statistical Analysis

Data from different groups were tested by the *t*-test for the significance of the difference between the means of two independent samples using the computer software KaleidaGraph (version 3.6, Synergy Software, Inc., Pennsylvania, PA).

RESULTS

Female Fertility Impaired by CD81 Deficiency

Figure 1A depicts the average litter size in matings of three genotypes of females, wild-type, CD81+/− and CD81−/− mice, with CD81+/− males over a period of 6 months. Although these females displayed normal mating behavior with the males (data not shown), the average litter size of CD81−/− females was markedly reduced relative to those of CD81+/− and wild-type mice (on average, 1.3 ± 2.5 vs. 11.3 ± 1.3 and 11.0 ± 0.8) (Fig. 1A). To examine the oocyte maturation and ovulation, we also collected the eggs from mice superovulated by stimulation with exogenous gonadotropin. The eggs collected from CD81−/− mice were indistinguishable with regard to morphology and number (on average, 18.0 ± 2.8) from those wild-type and CD81+/− mice (on average, 19.9 ± 1.7 and 21.7 ± 2.8) (Fig. 1B). Therefore, the reduction in fertility of CD81−/− females did not seem to be due to defects of ovulation or oocyte maturation.

Involvement of CD81 in Fertilization

To clarify the cause of the reduced fertility of CD81−/− females, the function of CD81−/− eggs was further examined by IVF. When cumulus oocyte complexes (COCs) collected from CD81−/− or wild-type control mice were incubated with the wild-type sperm, the sperm could disperse cumulus cells, somatic cells surrounding eggs, and reach and apparently penetrate the zona pellucida of CD81−/− and wild-type eggs. However, the average rate of eggs developing to the two-cell stage was substantially decreased for CD81−/− eggs (on average, $15.0 \pm 2.5\%$) compared with that for wild-type eggs (on average, $65.0 \pm 10.8\%$) 24 hr after incubation with the sperm (Fig. 1D). Furthermore, in CD81−/− eggs, several sperm were observed in the perivitelline space (Fig. 1C). The delayed formation of two-cell embryos and the accumulation of more than one sperm within the perivitelline space in CD81−/− eggs demonstrate that CD81−/− eggs have impaired ability of fertilization. Subsequently, to examine the cause of the impaired fertilization, we performed IVF for CD81−/− eggs and wild-type eggs after the zona pellucida was removed using acid Tyrode solution (Fig. 2A,B). To measure the number of sperm fused with eggs, both types of eggs were preloaded with DAPI before incubation with wild-type sperm (Yamagata et al., 2002). One hour after insemination, estimation of the average number of sperm fused with one egg by measurement of DAPI fluorescence revealed that CD81−/− eggs showed a decreased number of fused sperm (on average, 1.21 ± 0.23) in comparison with the wild-type eggs (on average, 1.95 ± 0.27). Those results suggest that CD81 is involved in sperm–egg fusion, either directly or indirectly.

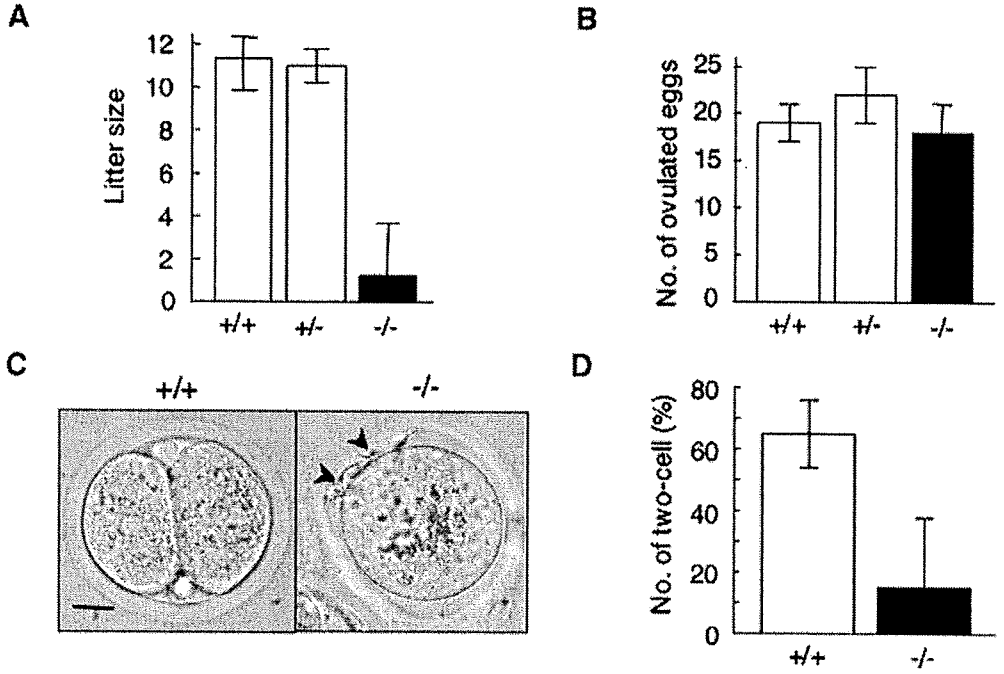

Fig. 1. Female infertility caused by CD81 deficiency. **A**: Average litter sizes of crosses between CD81+/− males and three types of females, wild-type, CD81+/− and CD81−/− mice. Each of the mating pairs was kept in a separate cage, and births over a 6-month period were monitored. Data of births during successive 2-month periods were grouped together, and the average litter size of wild-type, CD81+/− and CD81−/− females was calculated from data recorded for five mating pairs 8–15 weeks of age at the start of the experiment. **B**: Average number of ovulated eggs from wild-type, CD81+/− and CD81−/− female mice. The eggs were collected 13.5–16 hr after hCG treatment, and counted. **C**: Representative micrographs of CD81+/+ and CD81−/− eggs. The eggs were obtained 24 hr after incubation with the wild-type sperm. **D**: Average number of eggs that developed to the two-cell stage 24 hr after incubation with the wild-type sperm. The black bars show the results for CD81−/− eggs (A,B,D). Error bars represent SEM (A,B,D). Scale bar, 20 μm (C).

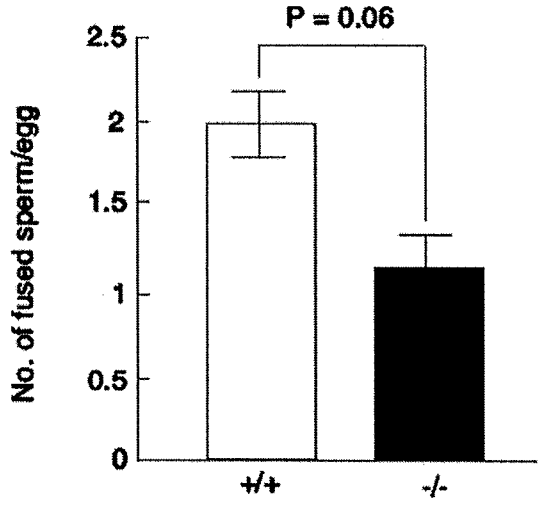

Fig. 2. In vitro sperm–egg fusion. Average number of sperm fused with wild-type or CD81−/− eggs after 3 hr of incubation. Error bars represent SEM. Data from different groups were tested by the *t*-test for the significance of the difference between the means of two independent samples ($P = 0.06$).

Expression of CD9 in CD81−/− Eggs

The mechanisms by which CD81 acts are still unclear. However, CD81 tends to form multimolecular complexes in which tetraspanins associate with specific proteins depending on the type of cell. In B cells, CD81 directly associates with CD19, taking part in the CD19-CD21-CD81 signaling complex (Pileri et al., 1998), which accords with the evidence that the expression of CD19 in bone marrow, spleen, and peripheral B cells is reduced in CD81−/− mice (Miyazaki et al., 1997). As previously mentioned, CD9 on the egg plasma membrane is required for fusion with sperm, and the impaired fusibility of CD81−/− eggs with sperm may likely be dependent on the expression of CD9. To investigate whether CD81 deficiency may cause downregulation of CD9 expression, the expression level of CD9 was examined (Fig. 3). We collected three types of eggs,

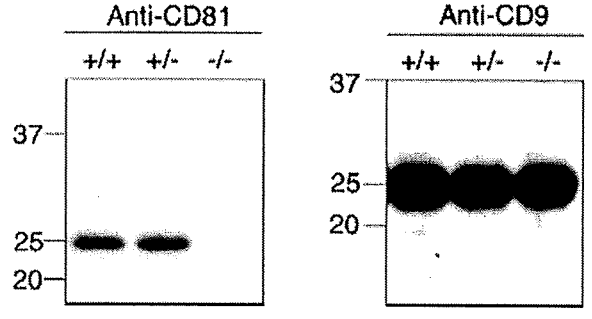

Fig. 3. The expression of CD9 in wild-type, CD81+/− and CD81−/− eggs. Proteins were isolated from the types of eggs indicated and resolved by sodium dodecyl sulfate polyacrylamide gel electrophoresis under nonreducing conditions. The proteins were electrophoretically transferred to a membrane, where they were probed with antibodies to CD81 (**panel A**) and CD9 (**panel B**). The proteins corresponding to each 110 egg (panel A) and 10 eggs (panel B) were analyzed.

wild-type, CD81+/− and CD81−/− eggs, 13.5–15 hr after hCG injection into mice, and examined the expression level of CD9 in comparison with that of CD81 by SDS–PAGE. The amounts of CD81 were invariable in wild-type and CD81+/− eggs, but CD81 was lost in CD81−/− eggs. By contrast, there were no significant differences in the expression of CD9 among these eggs. Therefore, the impairment of fertilization caused by CD81 deficiency cannot be attributed to decreased expression of CD9 in eggs.

Expression of CD81 During Folliculogenesis

The expression and localization of CD81 in ovarian tissues were immunohistochemically assessed using cryostat sections of adult wild-type ovaries. The follicles consist of immature eggs and granulosa cells that surround the egg; a single follicle usually grows to the preovulatory stage and releases the egg for potential fertilization (Buccione et al., 1990). Immunohistochemical staining with anti-CD81 mAb demonstrated that CD81 was continuously expressed in the egg and surrounding follicles (Fig. 4), and in cumulus cells surrounding ovulated eggs (data not shown). These data indicate that the sperm may encounter CD81 on the somatic cells surrounding eggs before direct interaction of sperm and eggs.

Possible Involvement of CD81 in Acrosome Reaction

Based on the localization of CD81 and the impaired fertilization of CD81−/− eggs, we speculated that the inability of wild-type sperm to fuse CD81−/− eggs might be due to impairment of prefusional stages, including the acrosome reaction. To examine the involvement of CD81 in the acrosome reaction of the sperm, CD81−/− eggs or wild-type eggs were incubated with the sperm collected from transgenic mice specifically expressing enhanced green fluorescent protein (EGFP) in the acrosomes (Fig. 5). The acrosome corresponds functionally to a lysosome and thus contains lysosomal enzymes (Moreno and Alvarado, 2006), and acrosin is a sperm acrosomal serine proteinase that is lost from the sperm head after the acrosome reaction is completed (Baba et al., 1994). Therefore, sperm expressing EGFP at the acrosomes in the heads are useful for the detection of acrosome-intact sperm. After 3 hr of incubation, we counted the number of acrosome-intact sperm within the perivitelline spaces. To count the sperm that had penetrated into the zona pellucida, the eggs were incubated with 3.0×10^5 sperm/ml. When the number of sperm within the perivitelline space were counted 3 hr after incubation with the eggs, we observed that an increased percentage ($8.5 \pm 2.3\%$) of the sperm that had penetrated into the perivitelline space of CD81−/− eggs exhibited EGFP fluorescence in their head portion. In contrast, very few sperm that had penetrated into the perivitelline space of wild-type eggs exhibited green fluorescence ($1.4 \pm 1.0\%$). These results suggest that the sperm that penetrated into the zona pellucida of the CD81−/− eggs were impaired in the acrosome reaction.

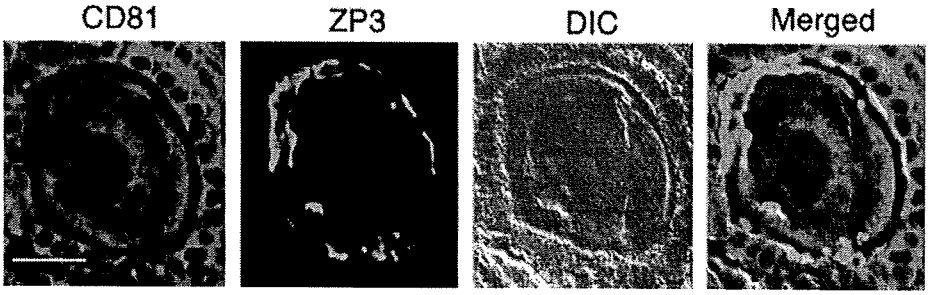

Fig. 4. CD81 is expressed at high levels in granulosa cells during oogenesis. Frozen sections of ovaries from wild-type mice were stained with anti-mouse CD81 mAb and with anti-ZP3 mAb. DIC represents a photograph taken by differential interference contrast. Scale bar, 20 μm. [See color version online at www.interscience.wiley.com.]

DISCUSSION

CD81 has been suggested to be a protein playing a role in membrane fusion events, but the function of CD81 in sperm–egg fusion remains unknown. As suggested by Rubinstein et al. (2006), CD9 and CD81 may have different roles in sperm–egg fusion. This notion is supported by the following facts: (1) deletion of a single gene, CD9 or CD81, causes impaired fertilization, and the expression of CD9 on eggs is not perturbed by CD81 deficiency, and (2) CD9−/− eggs injected with mRNA encoding CD81 cannot be fully rescued to the same degree as those injected with CD9 mRNA (Kaji et al., 2002).

Generally, the acrosome reaction is a change in the membrane of sperm that are activated for penetration into zona pellucida and facilitates the subsequent fusion with the egg membrane (Baba et al., 1994). During the acrosome reaction, the disruption of the acrosome covering the sperm head causes the release of acrosin and other proteolytic substances. As previously reported (Moreno and Alvarado, 2006), these materials included in the acrosome are important for the penetration of sperm into the zona pellucida and for sperm–egg fusion, but the molecular mechanism underlying the acrosome reaction is largely unknown. When wild-type eggs were incubated with sperm expressing EGFP in the acrosomes, we found the presence of acrosome-intact

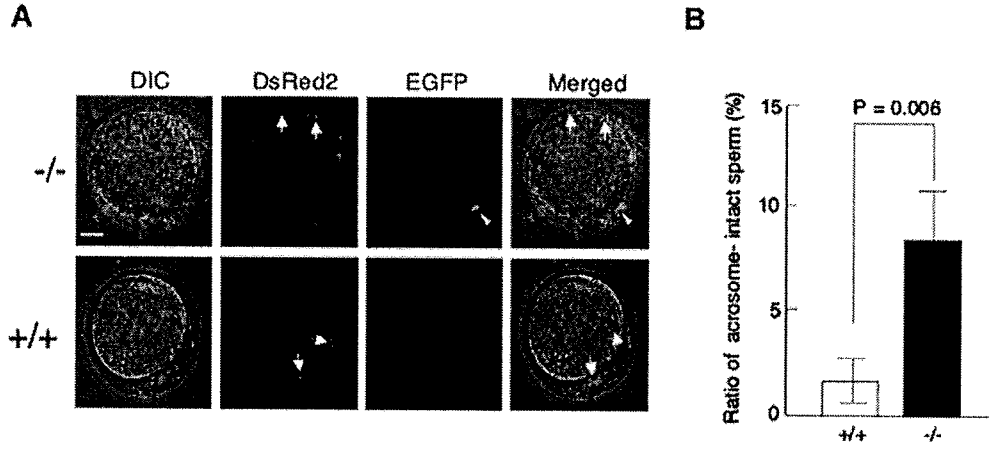

Fig. 5. In vitro fertilization assay for acrosome reaction. **A**: Representative photographs. CD81−/− eggs were incubated with transgenic sperm expressing EGFP at acrosomes in the sperm heads. Eggs from wild-type females were also subjected to fertilization using the AR-GFP transgenic sperm as controls. Four hours after insemination, the eggs were inspected for fluorescence using a confocal microscope. As shown in the **upper panel**, some CD81−/− eggs had sperm with green fluorescence (indicated by arrowheads) in their head region in the perivitelline space, while almost no wild-type eggs had such types of sperm (**lower panel**). Photomicrographs taken under light (DIC); photomicrographs taken for detecting DsRed2 translocated to mitochondria by the retention signal (Mt-DsRed2) and specifically expressed in the mid-piece of sperm (indicated by arrows); photomicrographs taken for detecting EGFP-derived green fluorescence specifically expressed in the head region of sperm (indicated by arrowheads); merged images. Scale bar, 20 μm. **B**: Examination of acrosome reaction using EGFP-expressing sperm. CD81−/− or wild-type eggs were fertilized in vitro with epididymal sperm expressing EGFP in the acrosomes. Four hours after insemination, the sperm entering into the perivitelline space were inspected for fluorescence using a confocal microscope. Note that the number of sperm carrying intact acrosomes (exhibiting green fluorescence in the sperm head region, as shown in A) and entering into the perivitelline space of CD81−/− eggs was significantly higher than that of acrosome-intact sperm entering into the perivitelline space of wild-type eggs. Acrosome-intact sperm can easily be detected since they exhibit bright green fluorescence in their head region. The total number of sperm entered into perivitelline space can be counted by inspection for red fluorescence in the mid-piece of the sperm. [See color version online at www.interscience.wiley.com.]

sperm in the outer layer of the zona pellucida (data not shown), but almost all sperm that penetrated into the perivitelline space had lost the acrosome caps (Fig. 5). These findings suggest that the acrosome reaction may occur in the perivitelline space and/or inner layer of the zona pellucida.

Another possible reason for the failure of the acrosome reaction of EGFP-expressing sperm in CD81−/− eggs is that "zona hardening" in CD81−/− eggs may not be sufficient compared to that in wild-type eggs. The weakened zona hardening might permit the penetration of some acrosome-intact sperm into CD81−/− eggs. However, since proteins other than components forming the zona pellucida may be triggers for preventing polyspermy and zona hardening (Sun, 2003), it would be of interest to test whether CD81 and ZP3 interact with each other.

In conclusion, the results of our IVF experiments suggest the possible involvement of CD81 in the acrosome reaction of zona pellucida-penetrated sperm prior to the fusion of sperm with eggs. Extensive attempts to elucidate the role of CD81 in the acrosome reaction are now underway.

ACKNOWLEDGMENTS

We are thankful for Dr. Tsujimoto (Faculty of Medicine, Osaka University) for kindly providing mt-DsRed2 contract for transgenic production. This work was supported by a grant from Precursory Research for Embryonic Science and Technology (PRESTO), The Ministry of Health, Labour and Welfare, and a grant-in aid for Scientific Research, The Ministry of Education, Culture, Sports, and Technology, of Japan.

REFERENCES

Baba T, Azuma S, Kashiwabara S, Toyoda Y. 1994. Sperm from mice carrying a targeted mutation of the acrosin gene can penetrate the oocyte zona pellucida and effect fertilization. J Biol Chem 269: 31845–31849.

Beebe SJ, Leyton L, Burks D, Ishikawa M, Fuerst T, Dean J, Saling P. 1992. Recombinant mouse ZP3 inhibits sperm binding and induces the acrosome reaction. Dev Biol 151:48–54.

Buccione R, Schroeder AC, Eppig JJ. 1990. Interactions between somatic cells and germ cells throughout mammalian oogenesis. Biol Reprod 43:543–547.

Cormier EG, Tsamis F, Kajumo F, Durso RJ, Gardner JP, Dragic T. 2004. CD81 is an entry coreceptor for hepatitis C virus. Proc Natl Acad Sci USA 101:7270–7274.

Deng J, Yeung VP, Tsitoura D, DeKruyff RH, Umetsu DT, Levy S. 2000. Allergen-induced airway hyperreactivity is diminished in CD81-deficient mice. J Immunol 165:5054–5061.

Higginbottom A, Quinn ER, Kuo CC, Flint M, Wilson LH, Bianchi E, Nicosia A, Monk PN, McKeating JA, Levy S. 2000. Identification of amino acid residues in CD81 critical for interaction with hepatitis C virus envelope glycoprotein E2. J Virol 74:3642–3649.

Kaji K, Oda S, Miyazaki S, Kudo A. 2002. Infertility of CD9-deficient mouse eggs is reversed by mouse CD9, human CD9, or mouse CD81; polyadenylated mRNA injection developed for molecular analysis of sperm-egg fusion. Dev Biol 247:327–334.

Kaji K, Oda S, Shikano T, Ohnuki T, Uematsu Y, Sakagami J, Tada N, Miyazaki S, Kudo A. 2000. The gamete fusion process is defective in eggs of Cd9-deficient mice. Nat Genet 24:279–282.

Le Naour F, Rubinstein E, Jasmin C, Prenant M, Boucheix C. 2000. Severely reduced female fertility in CD9-deficient mice. Science 287:319–321.

Miyado K, Yamada G, Yamada S, Hasuwa H, Nakamura Y, Ryu F, Suzuki K, Kosai K, Inoue K, Ogura A, Okabe M, Mekada E. 2000. Requirement of CD9 on the egg plasma membrane for fertilization. Science 287:321–324.

Miyazaki T, Muller U, Campbell KS. 1997. Normal development but differentially altered proliferative responses of lymphocytes in mice lacking CD81. EMBO J 16:4217–4225.

Moreno RD, Alvarado CP. 2006. The mammalian acrosome as a secretory lysosome: New and old evidence. Mol Reprod Dev 73:1430–1434.

Nakanishi T, Ikawa M, Yamada S, Parvinen M, Baba T, Nishimune Y, Okabe M. 1999. Real-time observation of acrosomal dispersal from mouse sperm using GFP as a marker protein. FEBS Lett 449:277–283.

Pileri P, Uematsu Y, Campagnoli S, Galli G, Falugi F, Petracca R, Weiner AJ, Houghton M, Rosa D, Grandi G, Abrignani S. 1998. Binding of hepatitis C virus to CD81. Science 282:938–941.

Rubinstein E, Ziyyat A, Prenant M, Wrobel E, Wolf JP, Levy S, Le Naour F, Boucheix C. 2006. Reduced fertility of female mice lacking CD81. Dev Biol 290:351–358.

Schwander M, Leu M, Stumm M, Dorchies OM, Ruegg UT, Schittny J, Muller U. 2003. Beta1 integrins regulate myoblast fusion and sarcomere assembly. Dev Cell 4:673–685.

Sun QY. 2003. Cellular and molecular mechanisms leading to cortical reaction and polyspermy block in mammalian eggs. Microsc Res Tech 61:342–348.

Tachibana I, Hemler ME. 1999. Role of transmembrane 4 superfamily (TM4SF) proteins CD9 and CD81 in muscle cell fusion and myotube maintenance. J Cell Biol 146:893–904.

Takahashi Y, Bigler D, Ito Y, White JM. 2001. Sequence-specific interaction between the disintegrin domain of mouse ADAM 3 and murine eggs: Role of beta1 integrin-associated proteins CD9, CD81, and CD98. Mol Biol Cell 12:809–820.

Takeda Y, Tachibana I, Miyado K, Kobayashi M, Miyazaki T, Funakoshi T, Kimura H, Yamane H, Saito Y, Goto H, Yoneda T, Yoshida M, Kumagai T, Osaki T, Hayashi S, Kawase I, Mekada E. 2003. Tetraspanins CD9 and CD81 function to prevent the fusion of mononuclear phagocytes. J Cell Biol 161:945–956.

Yamagata K, Nakanishi T, Ikawa M, Yamaguchi R, Moss SB, Okabe M. 2002. Sperm from the calmegin-deficient mouse have normal abilities for binding and fusion to the egg plasma membrane. Dev Biol 250:348–357.

DEVELOPMENTAL DYNAMICS 237:247–258, 2008

HB-EGF Decelerates Cell Proliferation Synergistically With TGFα in Perinatal Distal Lung Development

Seigo Minami, Ryo Iwamoto,* and Eisuke Mekada

Heparin-binding epidermal growth factor-like growth factor (HB-EGF) is a member of the EGF family of growth factors that is suggested to be involved in distal lung development. In HB-EGF null ($HB^{del/del}$) newborns, a histopathologic analysis revealed abnormally thick saccular walls occurring from embryonic day 18.5 that reduced the terminal saccular space area. HB-EGF gene deletion resulted in a significant increase in cell proliferation, indicating that HB-EGF suppresses distal lung cell proliferation. Furthermore, an analysis of saccular morphology and proliferation in HB-EGF and transforming growth factor-α (TGFα) double-mutant newborns revealed that HB-EGF and TGFα function synergistically in this suppression. Finally, crosses between $HB^{del/del}$ mice and waved 2 mice, a hypomorphic EGF receptor (EGFR) mutant strain, suggest that HB-EGF and EGFR cooperate in this process. Thus, HB-EGF has a novel suppressive function that contributes to decelerating distal lung cell proliferation synergistically with TGFα through EGFR in perinatal distal lung development. *Developmental Dynamics 237:247–258, 2008.*

Key words: HB-EGF; TGFα; EGFR; distal lung development

Accepted 4 November 2007

INTRODUCTION

In the mouse embryo, the development of the lung begins with the outpouching of an endodermal budding from the foregut at embryonic day (E) 9–9.5 (E9–E9.5). Mouse lung development comprises six different stages: the organogenesis (E9.5–E12), the pseudoglandular stage (E12–E16.5), the canalicular stage (E16.5–E17.5), the saccular stage (E17.5 to postnatal day 4 [P4]), the alveolization phase (P4–P14), and the phase of microvascular maturation (P14–P21) (Ten Have-Opbroek, 1991; Burri, 1999; Roth-Kleiner et al., 2004). The progression from canalicular to saccular stage is especially important for lung development, as terminal sacs and vascularization develop during the canalicular stage. Subsequently, the number of terminal sacs and vascularization rapidly increases in the saccular stage. In this stage, as interstitial tissue thins, the saccular spaces expand, the capillary network forms, and type I and II epithelial cells differentiate. Therefore, the saccular stage, which prepares the distal lung for subsequent alveolarization and

ABBREVIATIONS **E** embryonic day **P** postnatal day **EGF** epidermal growth factor **EGFR** EGF receptor **HB-EGF** heparin-binding EGF-like growth factor **TGFα** transforming growth factor-α **AR** amphiregulin **EPR** epiregulin **BTC** betacellulin **GAPDH** glyceraldehydes-3-phosphate dehydrogenase **PBS** phosphate-buffered saline **PCR** polymerase chain reaction **RT-PCR** reverse transcription-PCR **TSSA** terminal saccular space area **TUNEL** terminal deoxynucleotidyltransferase-mediated dUTP nick-end labeling **DAB** diaminobenzidine.

Department of Cell Biology, Research Institute for Microbial Diseases, Osaka University, Osaka, Japan
Grant sponsor: the Ministry of Education, Culture, Sports, Science, and Technology; Grant number: 18570176; Grant number: 18370079; Grant sponsor: Takeda Science Foundation.
***Correspondence to: Ryo Iwamoto, Department of Cell Biology, Research Institute for Microbial Diseases, Osaka University, 3-1, Yamadaoka, Suita, Osaka 565-0871, Japan. E-mail: riwamoto@biken.osaka-u.ac.jp**

DOI 10.1002/dvdy.21398
Published online 10 December 2007 in Wiley InterScience (www.interscience.wiley.com).

gas exchange upon parturition, is absolutely critical for normal lung development.

In normal lung development, epidermal growth factor receptor (EGFR) signaling is fundamentally established. EGFR null mice exhibit defective branching morphogenesis and saccular formation as well as immature differentiation of type II epithelial cells. These EGFR null mice die within a few days after birth, most likely due to respiratory failure caused by immature lung development (Miettinen et al., 1995, 1997; Sibilia and Wagner, 1995). Such molecular genetic studies demonstrate that EGFR signaling plays a crucial role during the saccular stage of lung development.

However, EGFR signaling is complex. The EGF-ErbB signaling network includes four related tyrosine kinase receptors, EGFR (ErbB1) and the ErbB receptors (ErbB2–4), and it also includes multiple ligands of the EGF/neuregulin superfamily (Holbro and Hynes, 2004). The EGF family ligands that bind to EGFR include EGF, transforming growth factor-α (TGFα), amphiregulin (AR), epiregulin (EPR), betacellulin (BTC), epigen, and heparin-binding EGF-like growth factor (HB-EGF) (Harris et al., 2003).

HB-EGF binds to and activates both EGFR and ErbB4 (Higashiyama et al., 1991; Elenius et al., 1997). HB-EGF is synthesized as a type I transmembrane protein (proHB-EGF), and as other EGF family ligands (Massague and Pandiella, 1993), proHB-EGF is cleaved at the juxtamembrane domain, resulting in the shedding of soluble HB-EGF (sHB-EGF; Goishi et al., 1995). sHB-EGF is a potent mitogen and chemoattractant for several cell types (Raab and Klagsbrun, 1997), while proHB-EGF acts as a juxtacrine growth factor that signals to adjacent neighboring cells in a nondiffusible manner (Iwamoto and Mekada, 2000).

HB-EGF has been implicated in several physiological and pathological processes (Raab and Klagsbrun, 1997). Importantly, analyses of HB-EGF null mice have shown that HB-EGF is a crucial factor for proper heart development and function (Iwamoto et al., 2003; Jackson et al., 2003; Yamazaki et al., 2003; Iwamoto and Mekada, 2006), eyelid development (Mine et al., 2005), skin wounding healing (Shirakata et al., 2005), and skin hyperplasia (Kimura et al., 2005). Notably, HB-EGF has been suggested to be involved in proper lung development, as HB-EGF null newborns exhibit saccular wall thickening, a decrease in the number of sacculi, and the immature differentiation of type II epithelial cells (Jackson et al., 2003). Still, a detailed understanding of the key mechanisms underlying such lung abnormalities remains unclear.

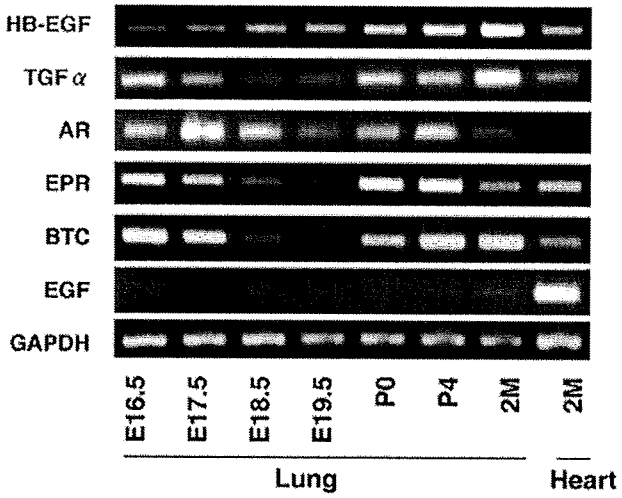

Fig. 1. Chronological analysis of EGFR ligands mRNA expression. RT-PCR of HB-EGF, TGFα, AR, EPR, BTC, EGF, and GAPDH mRNAs from mouse lung at the indicated stages (E16.5–adult) and heart (adult) was performed. For abbreviations, see list.

Therefore, to ascertain how HB-EGF regulates normal lung development, we used HB-EGF null mice to investigate how this specific EGFR ligand regulates cell proliferation in developing pulmonary tissue. Here, we present a novel mechanistic function for HB-EGF in saccular formation. Our data suggest that HB-EGF decelerates cell proliferation synergistically with TGFα selectively through EGFR signaling in perinatal distal lung development.

RESULTS

Postnatal Early Lethality of $HB^{del/del}$ Mice With C57BL/6J Background

We previously reported that approximately half of $HB^{del/del}$ mice with a mixed background (C57BL/6J, ICR, and CBA) show early lethality within a few weeks after birth. The survivors reach adulthood, but many gradually die around 2 to 3 months after birth, probably from heart failure (Iwamoto et al., 2003). In this study, however, we found that the $HB^{del/del}$ mice that have been back-crossed for more than eight generations onto a background of C57BL/6J strain almost all died within a few days after birth and rarely grew up (Fig. S1). No significant difference between $HB^{del/del}$ and $HB^{+/+}$ newborns was noted in body weight ($HB^{del/del}$: 1.42 ± 0.07 g, n = 7 vs. $HB^{+/+}$: 1.38 ± 0.05 g, n = 8; P = 0.67). Although we did not find any abnormalities in our $HB^{del/del}$ lungs with the mixed background of C57BL/6J, ICR and CBA, it has been reported that HB-EGF null mice with the mixed background of C57BL/6J and 129/Sv strains exhibit developmental abnormality in lung (Jackson et al., 2003). We did not detect any obvious histological abnormalities in lung development during pseudoglandular and canalicular stages with the $HB^{del/del}$ mice in C57BL/6J background (data not shown). These observations suggest that any developmental abnormality in lung occurring during the perinatal stage might be a major cause of the perinatal lethality of our $HB^{del/del}$ mice with C57BL/6J background. Therefore, we investigate here the HB-EGF function in lung development, especially focusing on the

perinatal saccular stage, by using $HB^{del/del}$ mice with a C57BL/6J background.

HB-EGF Expression Is Sustained During Prenatal Saccular Stage

First, we performed a chronological analysis of mRNA expression of EGFR ligands including HB-EGF in the lung during canalicular to perinatal saccular stage by reverse transcription-polymerase chain reaction (RT-PCR; Fig. 1). All of the EGFR ligands except EGF have already commenced expression by E16.5. At this stage, however, HB-EGF expression was extremely low when compared with the other EGFR ligands. Expressions of TGFα, AR, EPR, and BTC decreased markedly from E18.5 to E19.5, while only HB-EGF expression was sustained and gradually increased during this stage. Subsequently, expression of all the EGFR ligands except for EGF were increased rapidly just after birth. These chronological expression profiles of EGFR ligands suggest that only HB-EGF is a major factor among EGFR ligands in the developing prenatal lung.

HB-EGF Is Expressed in Lung Alveolar Epithelial Cells

To examine the expression pattern of HB-EGF in lung development, a targeting vector containing the *LacZ* reporter gene for HB-EGF expression was used (Iwamoto et al., 2003). *LacZ*-positive cells were detected in a manner of scattered distributions both in epithelial and interstitial cells of $HB^{del/+}$ and $HB^{del/del}$ newborns and $HB^{del/+}$ adult lungs (Fig. 2). Vascular endothelial cells (as indicated in Fig. 2B) and large bronchial epithelial cells (data not shown) were negative for *LacZ* detection. Although RT-PCR analysis showed HB-EGF expression in lung of the canalicular stage (Fig. 1), we could not detect *LacZ*-positive cells clearly in lung sections of prenatal embryos (data not shown). This disparity might be due to less sensitivity of *LacZ*-staining to that of RT-PCR. The observed pattern of HB-EGF expression in lung suggests that HB-EGF may participate in lung saccular and alveolar development and maintenance of mature lung formation.

Lungs Lacking HB-EGF Exhibit Abnormally Thickened Morphology in Saccular Walls During Saccular Stage

Therefore, to investigate the role of HB-EGF in distal lung development, we examined the morphology of distal lungs in $HB^{del/del}$ embryos and newborns during the saccular stage. $HB^{del/del}$ lungs exhibited an abnormally thickened morphology in saccular walls, an increased number of cells in the saccular septae, and poorly inflated sacculi in parts when compared with wild-type lungs (Fig. 3A). These abnormalities were observed in more than half of the newborn $HB^{del/del}$ lungs. Although $HB^{del/del}$ mice are known to exhibit enlarged cardiac valves and cardiac hypertrophy, these lung phenotypes were obviously not caused by pulmonary edema due to severe heart failure, based on the following observations; first, saccular septae were not edematous histologically. Second, no significant difference between $HB^{del/del}$ and $HB^{+/+}$ lungs were found in wet-to-dry lung weight ratio ($HB^{del/del}$: 5.32 ± 0.23, $n = 7$ vs. $HB^{+/+}$: 5.63 ± 0.15, $n = 8$; $P = 0.27$).

To analyze quantitatively these developmental abnormalities in $HB^{del/del}$ lungs, the terminal saccular space areas (TSSA) were measured (Shi et al., 1999; Zhao et al., 2001; Yu et al., 2004). In this analysis, a decrease of TSSA represents an increase of thickness of saccular walls and/or a decrease of saccular inflation. As a result, TSSA was significantly reduced in $HB^{del/del}$ lungs at E18.5, E19.5, and postnatal day (P) 0, but not at E17.5, when compared with those of wild-type lungs at each stage (Fig. 3B). Thus, the abnormalities in $HB^{del/del}$ lung saccular morphology occurred from E18.5 and were remarkable especially at birth (Fig. 3B). These results indicate that HB-EGF is involved in normal distal lung formation during the perinatal saccular stage.

Although it has been reported that the HB-EGF null lung presents an immature differentiation in sacculi (Jackson et al., 2003), our immunohistochemical analysis revealed no remarkable change in the expression of pro-surfactant protein C, a marker for the differentiated type II epithelial cells, between $HB^{+/+}$ and $HB^{del/del}$ lung sacculi (Fig. 4), suggesting that the observed abnormality in lung sacculi of our $HB^{del/del}$ mice is not due to defects in differentiation of saccular epithelium.

HB-EGF Contributes to Deceleration of the Distal Lung Cell Proliferation

Next, we examined whether the thickening of the saccular walls in $HB^{del/del}$ lungs is due to an increased proliferation or to a reduced apoptosis of the distal lung cells. Thus, cell proliferation and apoptosis in distal lungs during perinatal saccular were examined by immunohistochemistry of Ki67, a proliferation marker, and terminal deoxynucleotidyltransferase-mediated dUTP nick-end labeling (TUNEL) staining, respectively.

In distal lungs of E19.5 $HB^{del/del}$ embryos, a significantly increased number of Ki67-positive cells was detected compared with wild-type (Fig. 5A). Consistent with the TSSA analysis (Fig. 3B), in each stage of E18.5 to P0, the ratio of Ki67-positive cells to total cells was significantly increased in $HB^{del/del}$ lung, compared with that of wild-type (Fig. 5B). Moreover, while in the wild-type lung the ratio of Ki67-positive cells had gradually decreased during the perinatal saccular stage, in $HB^{del/del}$ lungs the higher ratio of Ki67-positive cells remained until E19.5 (Fig. 5B). On the other hand, only a few TUNEL-positive cells were detected both in wild-type and $HB^{del/del}$ lungs during this stage, and there was no significant difference in the ratio of TUNEL-positive cells to total cells between wild-type and $HB^{del/del}$ lungs (Fig. 5C,D). These results indicate that abnormally thickened saccular walls in $HB^{del/del}$ lungs is due to increased proliferation, but not to reduced apoptosis, in the distal lung cells and that HB-EGF contributes to the deceleration of such distal lung cell proliferation.

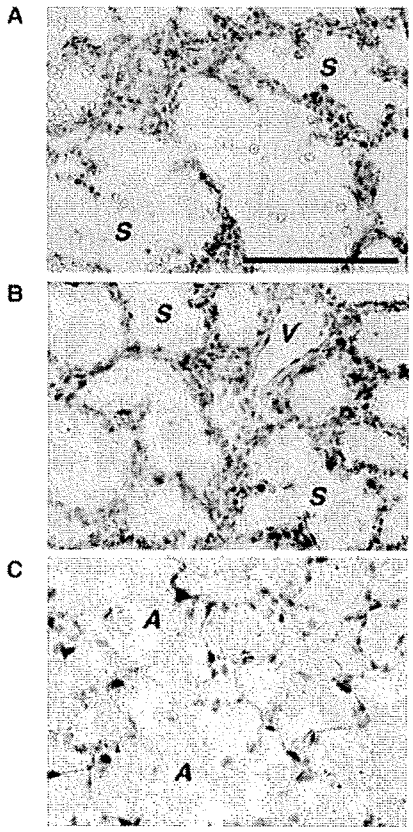

Fig. 2. HB-EGF expression in newborn lung sacculi. *LacZ* staining of (**A**) $HB^{del/+}$ newborn lung, (**B**) $HB^{del/del}$ newborn lung, and (**C**) $HB^{del/+}$ 2-month-old lung. The *LacZ*-stained tissues were counterstained with nuclear fast red. Original magnification: ×400. V, vessel; S, sacculus; A, alveolus. For other abbreviations, see list. Scale bar = 100 μm.

HB-EGF Functions Synergistically With TGFα in Perinatal Distal Lung Development

Recently, we have reported on the synergistic functions of HB-EGF and TGFα in the mouse eyelid closure pro-

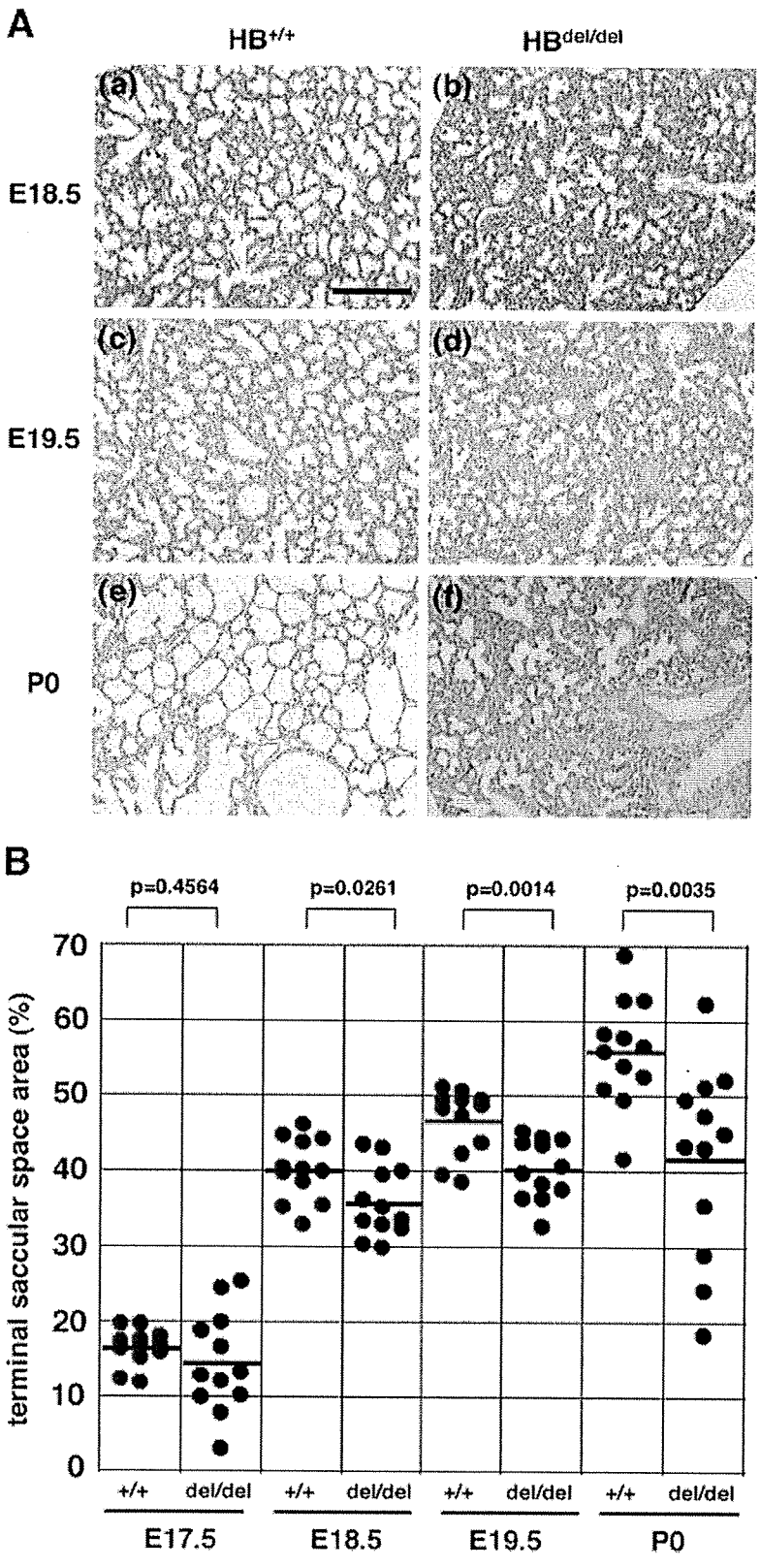

Fig. 3.

Fig. 3. Comparison of embryonic and newborn pup lung morphology between $HB^{del/del}$ and $HB^{+/+}$ genotypes. **A:** Representative hematoxylin/eosin-stained sections of lungs from $HB^{+/+}$(a,c,e) and $HB^{del/del}$ (b,d,f) at E18.5 (a,b), E19.5 (c,d), and newborn (P0) (e,f). **B:**Comparison of TSSA of $HB^{del/del}$ and $HB^{+/+}$ lungs. Each dot represents the percentage of TSSA from a single embryo or a newborn pup, with the horizontal lines representing the mean value for each genotype (n = 12). For abbreviations, see list. Original magnification, ×100. Scale bar = 200 μm in A.

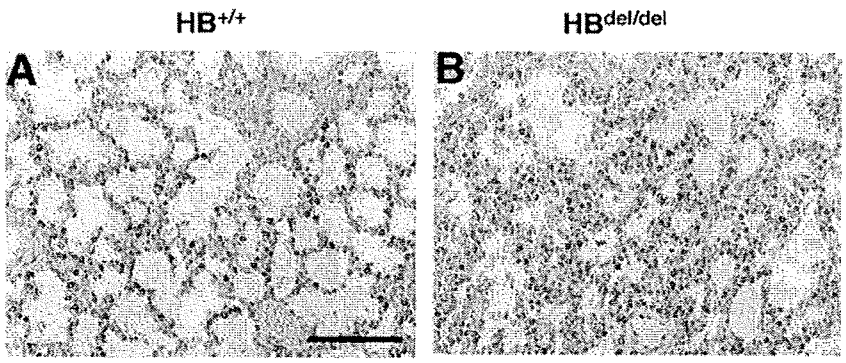

Fig. 4. Immunohistochemistry for pro-surfactant protein C. **A,B:** Sections of $HB^{+/+}$ (A) and $HB^{del/del}$ (B) newborn lung sacculi were immunostained for pro-SpC, a marker for type II epithelial cells. For abbreviations, see list. Original magnification, ×200. Scale bar = 100 μm.

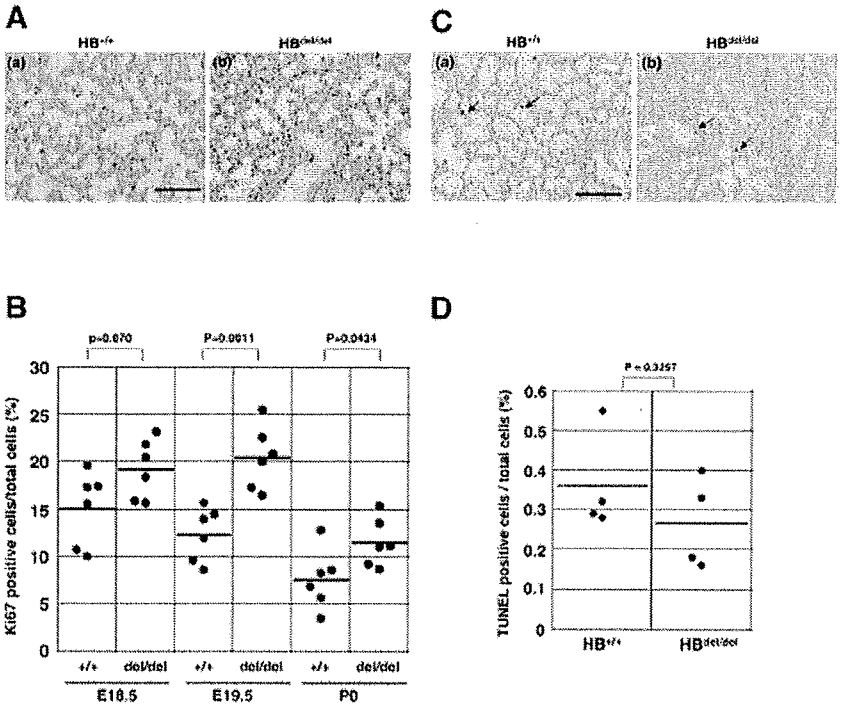

Fig. 5. Comparison of cell proliferation and apoptosis in embryonic and newborn pup lungs from $HB^{del/del}$ and $HB^{+/+}$ genotypes. **A:** Representative sections of $HB^{+/+}$ (a) and $HB^{del/del}$ (b) lungs at E19.5 immunostained for Ki67. **B:** Comparison of percentage of Ki67-positive cells in total lung cells at E18.5, E19.5, and newborn (P0). Each dot represents the percentage of Ki67-positive cells/total cells from a single embryo or a newborn pup, with the horizontal lines representing the mean value for each genotype (n = 6). **C:** Representative TUNEL-stained sections of $HB^{+/+}$ (a) and $HB^{del/del}$ (b) lungs at E19.5. Arrows indicate TUNEL-positive cells. **D:** Comparison of TUNEL-positive cell in lung saccular cells at E19.5. Each dot represents the percentage of TUNEL-positive cells/total cells from a single embryo, with the horizontal lines representing the mean value for each genotype (n = 4). For abbreviations, see list. Original magnification, ×200. Scale bar = 100 μm in A,C.

cess (Mine et al., 2005). Although lung abnormalities have not been reported in TGFα null mice to date, conditional prenatal overexpression of TGFα resulted in abnormal lung morphology at birth (Kramer et al., 2007), suggesting that proper expression of TGFα in lung is important for normal perinatal lung development.

As the expression of TGFα is regulated by HB-EGF in an autocrine manner in keratinocytes (Hashimoto et al., 1994; Piepkorn et al., 1998), we examined whether the defects in lung saccular development in $HB^{del/del}$ lungs were affected by changes in TGFα expression level. Major changes in the level of TGFα expression were not detected between wild-type and $HB^{del/del}$ lungs; however, the level of TGFα might even be somewhat slightly higher in the $HB^{del/del}$ lungs. Likewise, no significant difference was detected in the level of HB-EGF expression between wild-type and $TGF\alpha^{-/-}$ lungs (Fig. S2).

To test for a functional relationship between HB-EGF and TGFα in perinatal lung development, we examined double-null mutants of TGFα and HB-EGF. We tried to breed HB-EGF and TGFα double-null mice; however, intercrosses of $HB^{del/+}$; $Tgf\alpha^{+/-}$ double-heterozygous male and female mice could not produce any $HB^{del/del}$; $Tgf\alpha^{-/-}$ homozygous double-null newborns (in total 260 newborns from 39 litters). Thus, we compared $HB^{del/del}$; $Tgf\alpha^{+/+}$ and $HB^{+/+}$; $Tgf\alpha^{-/-}$ single homozygous null lungs with $HB^{del/del}$; $Tgf\alpha^{+/-}$ and $HB^{del/+}$; $Tgf\alpha^{-/-}$ lungs, respectively, of newborns. First, the TSSA in $Tgf\alpha^{-/-}$ single null lungs was significantly reduced compared with that of wild-type (Fig. 6A,B), indicating that TGFα also contributes to perinatal distal lung development. Then, TSSA was significantly reduced in $HB^{del/del}$; $Tgf\alpha^{+/-}$ lungs compared with $HB^{del/del}$; $Tgf\alpha^{+/+}$ lungs (Fig. 6A,B). On the other hand, TSSA in $HB^{del/+}$; $Tgf\alpha^{-/-}$ lungs was reduced slightly compared with $HB^{+/+}$; $Tgf\alpha^{-/-}$ lungs, without statistical significance. Scattering profiles of TSSA suggest that these differences were due to the increased penetrance, rather than severity, of the TSSA reduction.

Then, regarding proliferation rate of the distal lung cells, the ratio of Ki67-positive cells to the total cells was significantly increased in $HB^{del/del}$; $Tgf\alpha^{+/-}$ and $HB^{del/+}$; $Tgf\alpha^{-/-}$ lungs compared with $HB^{del/del}$; $Tgf\alpha^{+/+}$ and $HB^{+/+}$; $Tgf\alpha^{-/-}$ lungs, respectively. $HB^{+/+}$; $Tgf\alpha^{-/-}$ single null lungs also showed higher ratio of Ki67-positive cells than that of $HB^{+/+}$; $Tgf\alpha^{+/+}$ wild-type lungs, although not statistically significant (Fig. 6C,D).

These results strongly suggest that TGFα also contributes to deceleration of the distal lung cells in a relatively weaker manner than HB-EGF, and

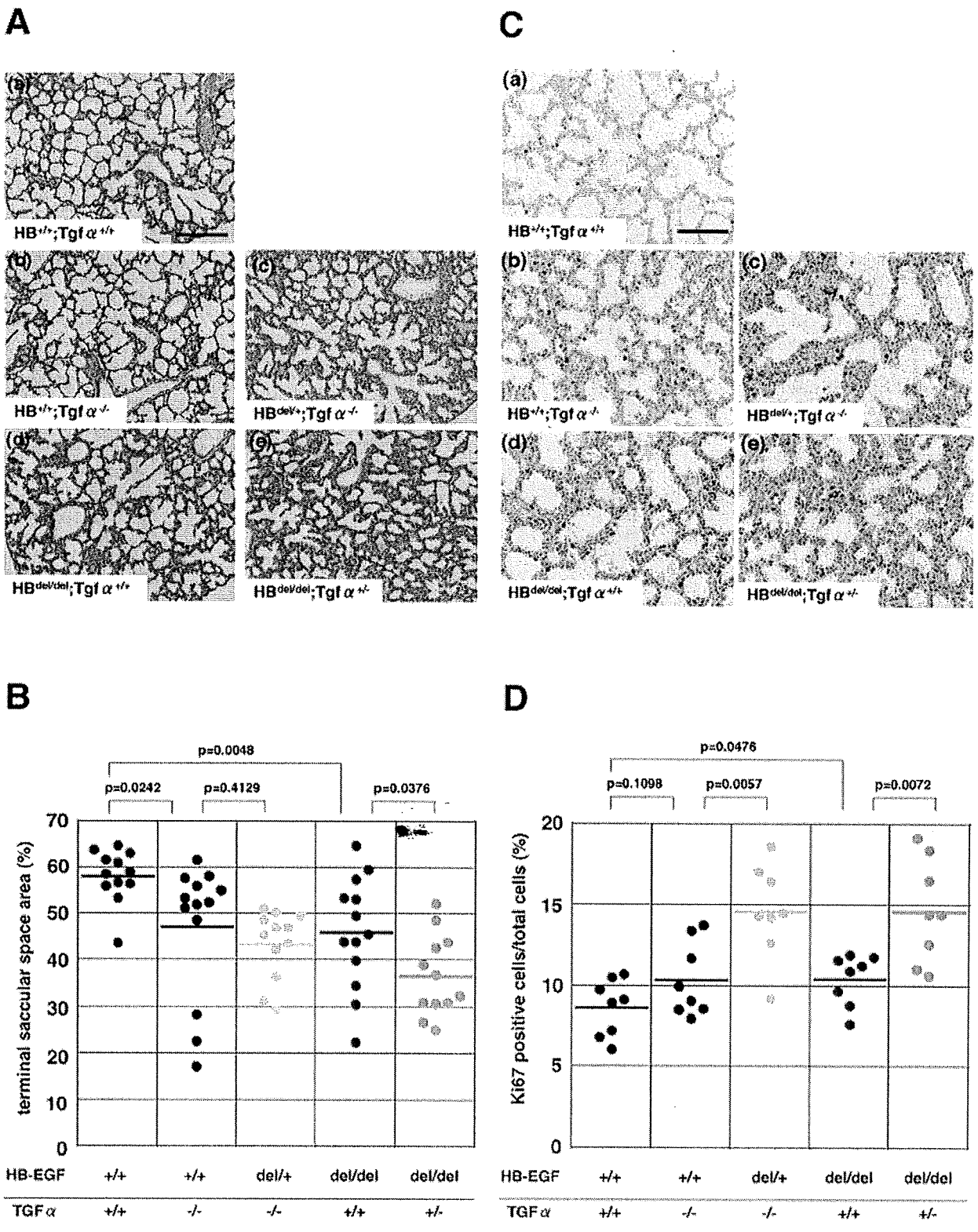
A
(a)
HB+/+;Tgfα+/+
(b)
HB+/+;Tgfα-/-
(c)
HBdel/+;Tgfα-/-
(d)
HBdel/del;Tgfα+/+
(e)
HBdel/del;Tgfα+/-
C
(a)
HB+/+;Tgfα+/+
(b)
HB+/+;Tgfα-/-
(c)
HBdel/+;Tgfα-/-
(d)
HBdel/del;Tgfα+/+
(e)
HBdel/del;Tgfα+/-
B
p=0.0048
p=0.0242
p=0.4129
p=0.0376
terminal saccular space area (%)
70
60
50
40
30
20
10
0
HB-EGF +/+ +/+ del/+ del/del del/del
TGFα +/+ -/- -/- +/+ +/-
D
p=0.0476
p=0.1098
p=0.0057
p=0.0072
Ki67 positive cells/total cells (%)
20
15
10
5
0
HB-EGF +/+ +/+ del/+ del/del del/del
TGFα +/+ -/- -/- +/+ +/-

Fig. 6.

that HB-EGF and TGFα function synergistically in perinatal distal lung formation.

EGFR Is Involved in HB-EGF–Dependent Perinatal Distal Lung Development

EGFR is a receptor for both HB-EGF and TGFα (Harris et al., 2003) and is essential for normal lung development (Miettinen et al., 1995; Sibilia and Wagner, 1995). To determine whether EGFR acts as a receptor for HB-EGF in perinatal distal lung development, we used a hypomorphic EGFR mutant, waved 2, and tested for a genetic interaction with HB-EGF. In waved 2 mice, the kinase activity of EGFR is decreased to less than 10% that of wild-type EGFR, owing to a point mutation in the kinase domain (Luetteke et al., 1994; Fowler et al., 1995). Because intercrosses of $HB^{del/+}$; wa2/+ double-heterozygous male and female mice produced only 3 $HB^{del/del}$; wa2/wa2 double-homozygous newborn (in total 234 newborns from 36 litters), we statistically compared $HB^{del/del}$; wa2/+ and $HB^{del/+}$; wa2/wa2 lungs with $HB^{del/del}$; +/+ and $HB^{+/+}$; wa2/wa2 lungs, respectively, of newborns. Reduction of the TSSA in $HB^{+/+}$; wa2/wa2 single mutant compared with that in wild-type is significantly remarkable. Reduction of TSSA in $HB^{del/del}$; wa2/+ lungs was more frequent than that of $HB^{del/del}$; +/+, although not statistically significant (Fig. 7A,B). We could not detect remarkable differences in the other comparative combinations (Fig. 7A,B).

Regarding proliferation rates, the ratio of Ki67-positive cells to the total cells was significantly increased in $HB^{del/del}$; +/+ and $HB^{+/+}$; wa2/wa2 lungs compared with $HB^{+/+}$; +/+ wild-type lungs. A comparison of the ratio of Ki67-positive cells between $HB^{+/+}$; wa2/wa2 and $HB^{del/+}$; wa2/wa2 lungs showed no significant difference. On the other hand, $HB^{del/del}$; wa2/+ lungs showed a relatively higher ratio of Ki67-positive cells than $HB^{del/del}$; +/+ lungs, although not statistically significant (Fig. 7C,D). Although the statistical significance in this study was lower than those of the case of HB-EGF and TGFα double mutants, these results suggest that EGFR is involved in the inhibitory function of HB-EGF in perinatal distal lung development.

DISCUSSION

We demonstrate here a novel role for HB-EGF in perinatal distal lung development. Our major findings are as follows: (1) HB-EGF is expressed in the lung epithelium and interstitium, and the mRNA level is gradually increased during the canalicular to perinatal saccular stage; (2) HB-EGF contributes to deceleration of perinatal cell proliferation in the distal lung; (3) HB-EGF functions synergistically with TGFα in this stage; (4) EGFR is involved in the HB-EGF function.

Although it has been previously reported that HB-EGF null newborns exhibit abnormal lung morphology (Jackson et al., 2003), the detailed information of such abnormality remains unclear. In this study, we demonstrate using HB-EGF null embryos and newborns that HB-EGF contributes to the deceleration of cell proliferation in the perinatal distal lung, based on the following findings: (1) $HB^{del/del}$ lungs showed significantly lower TSSA scores during perinatal saccular stage after E18.5 as compared to wild-type lungs; (2) in $HB^{del/del}$ lungs, the ratio of Ki67-positive cells in distal lungs was significantly higher than wild-type lungs in each stage examined; (3) only a few apoptotic cells were observed in the lungs in this stage, and no significant difference was detected between wild-type and $HB^{del/del}$ lungs. In this study, the possibility that HB-EGF is also involved in the lung inflation after birth cannot be ruled out; however, the major cause in the abnormally thick saccular walls in HB-EGF null lungs might be due to hypercellularity, because the rate of cell proliferation was significantly increased in the HB-EGF null lungs. Therefore, HB-EGF has an inhibitory function for cell proliferation in distal lungs during perinatal normal lung development. Consequently, the absence of HB-EGF resulted in the persistent deregulated hyperproliferative state in the distal lung cells. It is noteworthy that the ratio of Ki67-positive cells was decreased at birth even in $HB^{del/del}$ lungs, suggesting that there are some other factor(s) compensating HB-EGF functions, as discussed later.

HB-EGF has conventionally been thought of as a growth factor. Indeed, several lines of evidence point to a fundamental role for HB-EGF in cell proliferation and tumorigenesis (Miyamoto et al., 2006). However, no hypoplastic abnormalities have been found in HB-EGF null mice to date; rather, HB-EGF null mice exhibit hyperplastic abnormalities (Iwamoto et al., 2003; Jackson et al., 2003; Yamazaki et al., 2003; Iwamoto and Mekada, 2006) as well as defects in cell migration (Mine et al., 2005; Shirakata et al., 2005). These findings suggest that HB-EGF may not function as a growth factor in developmental and physiological processes. Importantly among these studies, the inhibitory function of HB-EGF for cell proliferation in vivo has also been reported in cardiac valve development (Iwamoto et al., 2003; Jackson et al., 2003; Yamazaki et al., 2003; Iwamoto and Mekada, 2006). In this process, HB-EGF is expressed only in the endocardial cells of developing cardiac valves, mainly during valve remodeling, and causes the inhibition of mesenchymal cell proliferation during valve remodeling. The molecular mechanisms that are involved in the inhibitory function of HB-EGF in both

Fig. 6. Comparison of TSSA and cell proliferation in double mutants of HB-EGF and TGFα newborn pups. **A:** Representative hematoxylin/eosin-stained sections of newborn lungs from $HB^{+/+}$;$Tgf\alpha^{+/+}$ (a), $HB^{+/+}$;$Tgf\alpha^{-/-}$ (b), $HB^{del/+}$;$Tgf\alpha^{-/-}$ (c), $HB^{del/del}$;$Tgf\alpha^{+/+}$ (d), and $HB^{del/del}$;$Tgf\alpha^{+/-}$ (e). **B:** Comparison of TSSA of newborn lungs from $HB^{+/+}$;$Tgf\alpha^{+/+}$, $HB^{+/+}$;$Tgf\alpha^{-/-}$, $HB^{del/+}$;$Tgf\alpha^{-/-}$, $HB^{del/del}$;$Tgf\alpha^{+/+}$, and $HB^{del/del}$;$Tgf\alpha^{+/-}$. Each dot represents the percentage of TSSA from a single newborn pup, with the horizontal lines representing the mean value for each genotype (n = 12). **C:** Representative sections immunostained for Ki67 of newborn (P0) lungs from $HB^{+/+}$;$Tgf\alpha^{+/+}$ (a), $HB^{+/+}$;$Tgf\alpha^{-/-}$ (b), $HB^{del/+}$;$Tgf\alpha^{-/-}$ (c), $HB^{del/del}$;$Tgf\alpha^{+/+}$ (d), and $HB^{del/del}$;$Tgf\alpha^{+/-}$ (e). **D:** Comparison of percentage of Ki67-positive cells in total lung cells of newborn lungs from $HB^{+/+}$;$Tgf\alpha^{+/+}$, $HB^{+/+}$;$Tgf\alpha^{-/-}$, $HB^{del/+}$;$Tgf\alpha^{-/-}$, $HB^{del/del}$;$Tgf\alpha^{+/+}$ and $HB^{del/del}$;$Tgf\alpha^{+/-}$. Each dot represents the percentage of Ki67-positive cells/total cells from a single newborn pup, with the horizontal lines representing the mean value for each genotype (n = 8). For abbreviations, see list. Original magnification, ×200. Scale bar = 100 μm in A,C.